Electronic Supplementary Material (ESI) for Physical Chemistry Chemical Physics.

Synthesis and Photophysics of Gold(I) Alkynyls Bearing a Benzothiazole-2,7-Fluorenyl Moiety: A Comparative Study Analyzing Influence of Ancillary Ligand, Bridging Moiety, and Number of Metal Centers on Photophysical Properties

Joseph J. Mihaly,[a‡] Alexis T. Phillips,[b,e‡] David J. Stewart,[b,c] Zachary M. Marsh,[b,d] Christopher L. McCleese,[b,c] Joy E. Haley,[b] Matthias Zeller,[f] Tod A. Grusenmeyer,[b] and Thomas G. Gray[a,*]

[a]Department of Chemistry, Case Western Reserve University, 10900 Euclid Avenue, Cleveland, Ohio 44106, United States

[b]Air Force Research Laboratory, Materials and Manufacturing Directorate, Wright-Patterson Air Force Base, Dayton, Ohio 45433, United States

[c]General Dynamics Information Technology, 5000 Springfield Pike, Dayton, Ohio, 45431, United States

[d]Azimuth Corporation, 4027 Colonel Glenn Hwy. Suite 230, Beavercreek, OH United States 45431

[e]Southwestern Ohio Council for Higher Education, Dayton, Ohio, 45420, United States

[f]Department of Chemistry, Purdue University, West Lafayette Indiana, 47907, United States

Table of Contents:

I. Materials and Methods

General Considerations. All experimental procedures were carried out under an inert atmosphere of argon using standard Schlenk line techniques. Microanalyses (C, H, and N) were undertaken by Atlantic Microlab. Mass spectrometry was performed at the University of Cincinnati Mass Spectrometry facility. (Phosphine)gold(I) chlorides and (i-Pr_2NHC)AuCl were prepared according to literature procedures.[1] Benzathiazole Ligand was synthesized according to literature procedure.[2] Dry 2-propanol, benzene, dichloromethane, pentane, and cesium carbonate were purchased from Sigma Aldrich and used as received. ^{1}H NMR experiments were performed on a Bruker-500 Ascend Advanced III HD NMR spectrometer operating at 500.24 MHz. ^{1}H chemical shifts are reported in parts per million (δ) with integration and multiplicity (s = singlet, d = doublet, t = triplet, q = quartet, dd = doublet of doublets, dt = doublet of triplets, td = triplet of doublets, ddd = doublet of doublet of doublets, and m = muliplet), measured from tetramethylsilane (0 ppm) and are referenced to residual solvent in $CDCl_3$ (7.26 ppm). $^{31}P\{^1H\}$ NMR, chemical shifts were determined relative to concentrated H_3PO_4. Thermogravimetric analysis (TGA) of the Au(I) complexes were carried out using a TA Q500. Samples were heated at a ramp rate of 10 °C min^{-1} to a final temperature of 600 °C or 800°C. TGA experiments were run in air.

Instrumentation

Detailed discussions of our instrumentation and data treatment have been previously reported.[3,4] A Cary 5000 spectrophotometer was used to obtain ground-state UV/Vis absorption spectra. Luminescence spectra were obtained using an Edinburgh Instruments FLS980 spectrometer. Fluorescence quantum yields were obtained using an integrating sphere in the FLS980. Time-correlated single-photon counting was used to determine the fluorescence lifetimes, which were measured with an Edinburgh Instruments OB920 spectrometer. The samples were excited using a laser diode at 375 nm. Fluorescence was detected at the peak maximum of the emission reported in Table 2. All fluorescence lifetimes were collected in duplicate. The decay traces were fit using a reconvolution fit routine provided in the Edinburgh Instruments software. An example fluorescence lifetime fit for each of the Au-ABTF compounds is shown in *Figure S10*.

Phosphorescence lifetimes were excited at 348 nm using a xenon flashlamp with an average power of 60 W. The phosphorescence decay was collected at the maximum reported in Table 2. The phosphorescent lifetimes were collected in triplicate. All samples were deaerated using three freeze-pump-thaw degas cycles prior to data collection. The final vacuum pressure obtained inside the cells can be found in Table *S1.* An example phosphorescence lifetime fit for each of the Au-ABTF compounds is shown in *Figure S10*.

Nanosecond transient absorption and kinetics were collected using a Edinburgh Instruments LP920. Samples were excited at 355 nm using the frequency tripled output of an Nd:YAG laser. Delayed fluorescence and triplet-triplet annihilation measurements were collected using freeze-pump-thaw degassed samples, and aerated solutions were used to measure the excited state extinction coefficients. All experiments described above were performed at room temperature and collected in duplicate. The results are reported Table 3. An example of the delayed fluorescence data, relative actinometry data, and triplet-triplet annihilation data for each of the Au-ABTF compounds are shown in *Figures S14-16*.

Ultrafast transient absorption measurements were performed using a modified version of the femtosecond pump-probe UV-Vis spectrometer described elsewhere.[5] Samples were excited using the frequency doubled output of a cryogenically-cooled Ti:Sapphire regenerative amplifier (KM Labs Wyvern). Ultrafast data was collected in aerated toluene solutions in 2 mm pathlength cuvettes. Lifetime analysis was performed at 10 different wavelengths using the Ultrafast Systems LLC Surface Xplorer software package. The average lifetime values are reported in Table 3. An example of the fit obtained at a single wavelength is shown in *Figure S17.*

Absolute Luminescence Quantum Yields. An integrated sphere was used in the Edinburgh Instruments FLS980 spectrometer to determine the fluorescence quantum yields. A blank toluene solution was placed in the integrating sphere to measure the excitation intensity. The emission slits were set to 0.26 nm, and the excitation slits were adjusted to obtain 1 million counts on the PMT detector, where the final achieved excitation slit width was 5 nm. All samples were excited at 366 nm. The luminescence signals were collected from 280 – 600 nm using a 0.3 nm step size averaging three times for each trial. The excitation signal was integrated from 360 – 372 nm, and the fluorescence signal was integrated from where the toluene blank and the sample intersected to 600 nm. A dilute sample was also measured to correct for reabsorption, where the dilute sample was diluted by a factor of 10. The dilute fluorescence spectrum was tail matched to the concentrated fluorescence spectrum to calculate the magnitude of reabsorption in the samples. The average of two trials is reported in *Table 2,* and an example dataset obtained for a fluorescence quantum yield trial for each of the Au-ABTF compounds is shown in *Figure S11*.

Relative Luminescence Quantum Yields. Relative luminescence quantum yield measurements were used to determine intersystem crossing and phosphorescence quantum yields. Singlet oxygen phosphorescence was used to determine the lower limit of the intersystem crossing quantum yield of the samples. This method utilizes singlet oxygen phosphorescence resulting from energy transfer from the triplet state of the sample to estimate the intersystem crossing efficiency. Phenazine ($\Phi_\Delta = 0.83$) was dissolved in toluene and used as the reference standard.[6] The excitation wavelength used corresponds to the wavelength where the samples were absorbance matched in the ground state. Excitation and emission slit widths were set at 3.0 and 21.0 nm, respectively. The emission spectra were averaged 50 times using 1 nm steps and the results were integrated from 1250 – 1330 nm. Because the same solvent was used for both phenazine and Au-ABTF samples, the refractive index correction factor can be neglected. The triplet quantum yields reported in Table 2 represent the average value of two trials. An example of the singlet oxygen phosphorescence measurement obtained for each of the Au-ABTF compounds is shown in *Figure S13*.

The phosphorescence quantum yields were measured using Rhodamine 6G as the reference standard. The Au-ABTF samples were absorbance matched with Rhodamine 6G in the ground state at 348 nm. The luminescence spectra were collected from 450 – 700 nm using a 1 nm step size and an emission slit width of 0.50 nm. Rhodamine 6G's fluorescence in ethanol and Au-ABTF's phosphorescence in toluene was integrated from 500- 750 nm to determine the phosphorescence quantum yield of the sample. The fluorescence spectra of Rhodamine 6G was corrected for reabsorption. A quantum yield of 0.95 was applied to Rhodamine 6G[7] and an index of refraction correction was applied using refractive indices reported in *The Handbook of*

Photochemistry.[8] The absorption and luminescence spectra are reported in *Figure 4*. It is important to note that tailing fluorescence exists in the phosphorescence spectra for all samples which overestimates the phosphorescence quantum yield obtained. The average phosphorescence quantum yields reported in *Table 2* has some tailing fluorescence incorporated, representing the upper limit of the observable. An example of the phosphorescence quantum yield data obtained for each of the Au-ABTF compounds is shown in *Figure S12*.

Excited State Extinction Coefficients. The triplet excited state extinction coefficients of the complexes were determined using $[Ru(bpy)_3]^{2+}$ as a standard in the relative actinometry method.[9] The laser experiments utilizing $[Ru(bpy)_3]^{2+}$ were collected in aereated acetonitrile solution and the laser experiments using the Au-ABTF complexes were collected in aereated toluene. The samples were absorbance matched in the ground state at 355 nm, which was used as the excitation wavelength for all measurements. Three measurements for each sample were collected around 200, 150, and 100 μJ laser energies for each sample to ensure a linear dependence between the excited state absorbance and the incident laser power. The transient absorption signal obtained from $[Ru(bpy)_3]^{2+}$ was monitored at 370 nm. The detection wavelength used for the Au-ABTF complexes is the maximum reported in Table 3. The excited state extinction coefficient of $[Ru(bpy)_3]$ was found to be 20,800 M^{-1} cm^{-1} at 364 nm in water using literature values[10] for ground and triplet state extinction coefficients. However, $[Ru(bpy)_3]^{2+}$ was analyzed in acetonitrile, and it was assumed that $\Delta\varepsilon$ at the 370 nm maximum in acetonitrile corresponded to the maximum calculated value at 364 nm in water. The refractive index correction factor was determined using values from *The Handbook of Photochemistry*.[8] The experiment was performed in duplicate under aerated conditions. *Figure S*15 reports the ground state absorbance for all trials and the kinetic decay traces used to determine the excited state extinction coefficients that are reported in Table 1. The calculated excited state extinction coefficients were applied to the normalized transient spectra that was collected 50 ns after the laser pulse to obtain excited state extinction coefficients at all spectral wavelengths.

Delayed Fluorescence. Delayed fluorescence spectra were obtained from freeze-pump-thaw degassed samples in toluene. Various laser pulse energies were used to determine the delayed fluorescence intensity dependence on laser energy. The gate delay was set to 50 μs after the laser pulse with a gate width of 99 μs using 355 nm excitation. The fluorescence signal at each laser energy was averaged over multiple laser shots to increase the signal to noise ratio. The spectra were integrated from 375 – 525 nm to obtain the integrated fluorescence intensities which were then normalized to one using the maximum integrated intensity value. These values were used to create plots of the integrated fluorescence intensity vs. laser pulse energy for all Au-ABTF complexes. Double logarithm plots of the data are also reported for all of the complexes. *Figure 4* represents the data collected for Au-ABTF0, and *Figure S14* represents the data collected for Au-ABTF1 and Au-ABTF2.

Triplet-Triplet Annihilation Fitting. The expression used to evaluate the rate constant for triplet-triplet annihilation is shown below in Equation S1, where k_t is the rate constant for the intrinsic decay of the triplet excited state, k_{tt} is the triplet-triplet annihilation rate constant, and $[^3M^*]_0$ and $[^3M^*]_t$ are the concentrations of the triplet excited state at time zero and time t following the laser pulse, respectively.[11] The transient absorption decay traces obtained in ΔA units were converted to triplet concentration units using the excited state extinction coefficients obtained in previous experiments. The phosphorescence lifetimes were also previously determined for all three complexes. The value of k_t was calculated by taking the inverse of the phosphorescence lifetime value. This calculated value of k_t is held constant when fitting the triplet-triplet annihilation data. Under these conditions, the expression is reduced to a single variable fit (k_{tt}), as a reasonable values of $[^3M^*]_0$ are easily determined via comparison with the y-axis. The use of this method to fit the transient absorption decay data for Au-ABTF1 and Au-ABTF2 provided fits that were in excellent agreement with the data; however, fits of Au-ABTF0 provided poor values of r^2 and reduced χ^2. The data for Au-ABTF0 was refit with both k_t and k_{tt} as floating parameters. The fit results obtained for Au-ABTF0 are shown in Figure 4, and the fit results obtained for Au-ABTF1 and Au-ABTF2 are reported in *Figure S16.* Values of k_t and k_{tt} for all three complexes are summarized in Table 3. The values obtained from best fits of Au-ABTF0 transient absorption decay data return values of k_t that is approximately two times larger than the value determined from the inverse of the phosphorescence lifetime. We feel that these fit results are an accurate representation of the decay of the triplet states in excited samples of Au-ABTF0, as the triplet excited state lifetimes are on the order of hundreds of microseconds and the rate constant for triplet-triplet annihilation is close to the diffusion limit in toluene. These observations are in agreement with the results obtained for all of the other Au-BTF and Au-ABTF complexes.

$$[^3M^*]_t = \frac{[^3M^*]_0 e^{-k_T t}}{1 + [^3M^*]_0 \left(\frac{k_{TT}}{k_T}\right)\left(1 - e^{-k_T t}\right)} \qquad (S1)$$

Singlet Excited State Extinction Coefficient Determination. Singlet excited state excited state extinction coefficients were calculated using the 0 picosecond transient absorption spectrum obtained ultrafast transient absorption experiments. The Equation S2 below was used to determine the singlet excited state extinction coefficient:

$$\Delta\varepsilon_{S_1-S_n} = \Delta\varepsilon_{S_1-S_n} \frac{(\Delta A_{S_1-S_n})\Phi_T}{(\Delta A_{T_1-T_n})} \qquad (S2)$$

where $\Delta\varepsilon_{s1-sn}$ represents the singlet excited state extinction coefficient, $\Delta\varepsilon_{t1-tn}$ represents the triplet excited state extinction coefficient, ΔA_{s1-sn} is the change in absorbance at time zero, ΔA_{t1-tn} is the change in absorbance at 1000 ps, and ϕ_t is the triplet quantum yield. The triplet excited state extinction coefficient was previously determined using relative actinometry, and the triplet quantum yield was determined from singlet oxygen phosphorescence.

Rate Constant Determinations.

Following the determination of the fluorescence lifetime, fluorescence quantum yield, and the intersystem crossing quantum yield. All relevant rate constants can be determined by solving the series of Equations S3-S5.

$$\tau_{FL} = \frac{1}{k_r + k_{nr} + k_{ISC}} \qquad (S3)$$

$$\Phi_{FL} = \frac{k_r}{k_r + k_{nr} + k_{ISC}} \qquad (S4)$$

$$\Phi_{TRIPLET} = \frac{k_{ISC}}{k_r + k_{nr} + k_{ISC}} \qquad (S5)$$

II. Synthesis, NMR, Mass Spectrometry and Elemental Analysis

Au-ABTF2:

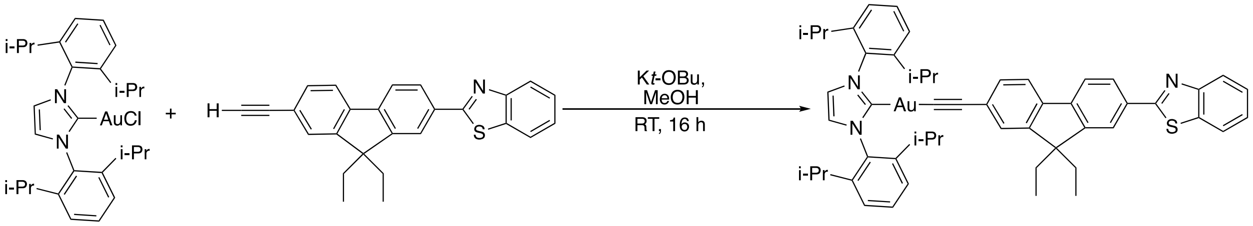

Prep: To a 20 mL scintillation vial equipped with a stir bar was added (23.5 mg, 0.322 mmol) of potassium *tert*-butoxide along with 4 mL of MeOH via syringe. The suspension was stirred until a solution was observed, after which (79.4 mg, 0.209 mmol) of BTF alkyne was added. Most didn't dissolve, so 3 mL of DCM was added creating a yellow solution. This solution was stirred at RT for 45 min and then transferred to another 20 mL scint. vial containing 2 mL of MeOH and (100 mg, 0.161 mmol) IPrAuCl, creating a yellow solution. This solution was stirred in the absence of light for 16 h and then concentrated *in vacuo*. The yellow solid was dissolved in dichloromethane, filtered over Celite, concentrated, and washed with (4 x 25 mL) of pentanes. The yellow solid was allowed to dry and then dissolved in hot ethanol and allowed to crystallize in a freezer at -10 ^{o}C. After two crops, 119 mg of yellow crystals were obtained. (76 % yield). ^{1}H NMR (500 MHz, Chloroform-*d*) δ 8.06 (d, *J* = 8.2 Hz, 1H), 8.03 (s, 1H), 7.96 (d, *J* = 9.3 Hz, 1H), 7.89 (d, 7.8 Hz, 1H), 7.66 (d, *J* = 8.0 Hz, 1H), 7.54-7.44 (m, 4H), 7.40-7.30 (m, 7H), 7.13 (s, 2H), 2.62 (sept, *J* = 6.8 Hz), 2.03 (m, *J* = 35.6, 13.6, 6.7 Hz, 4H), 1.41 (d, *J* = 6.8 Hz, 12H), 1.23 (d, *J* = 6.9 Hz, 12H), 0.21 (t, *J* = 7.3 Hz, 6H). HRMS (FT-ICR, $[M+H]^{+}$) m/z calcd for MH^{+} $C_{53}H_{57}AuN_{3}S^{+}$964.39339, found 964.39332 . Anal. Calcd for: $C_{53}H_{56}AuN_{3}S$: C, (66.03); H, (5.86); N, (4.36). Found: C, (65.80); H, (5.69); N, (4.37).

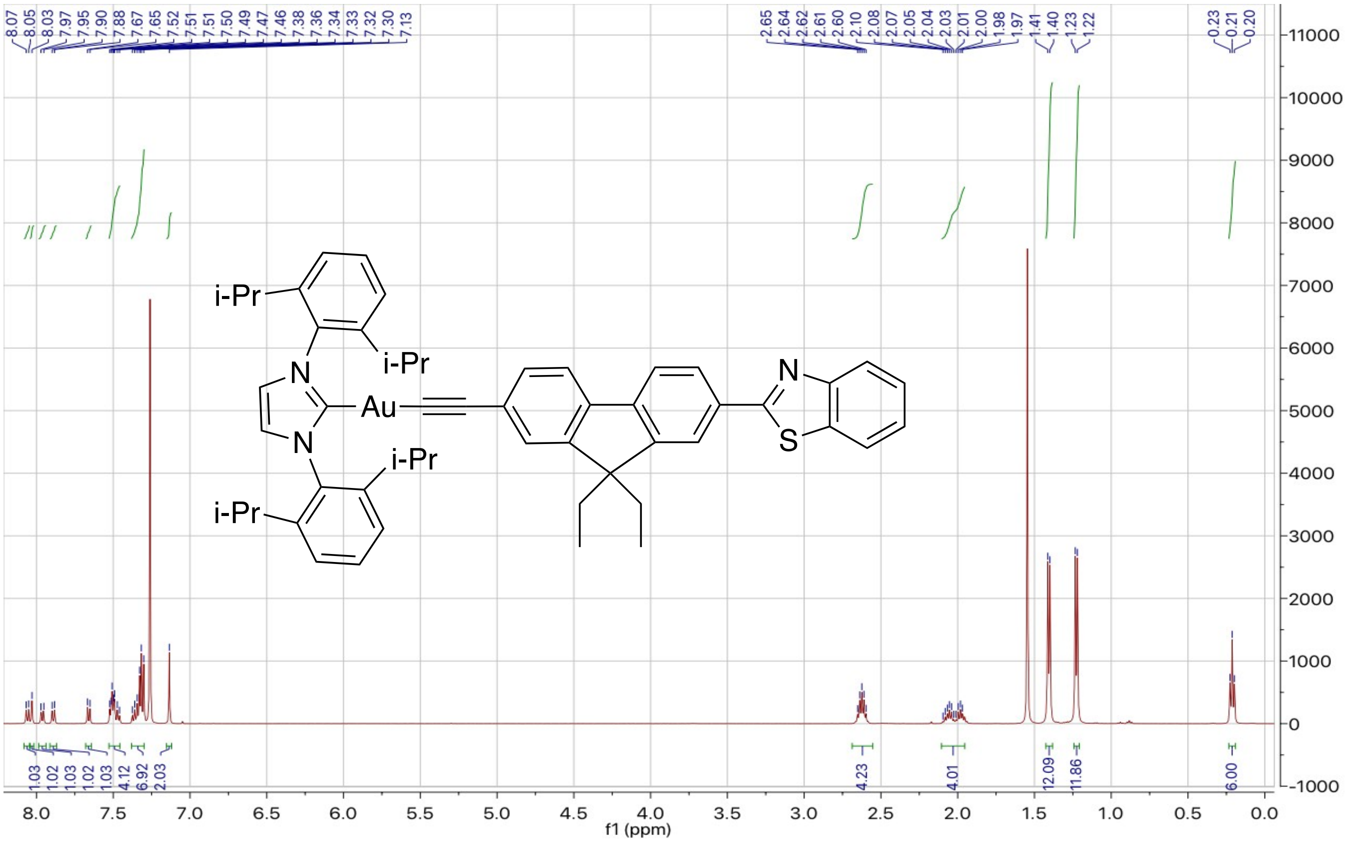

Figure S1: ^{1}H NMR of **Au-ABTF2**

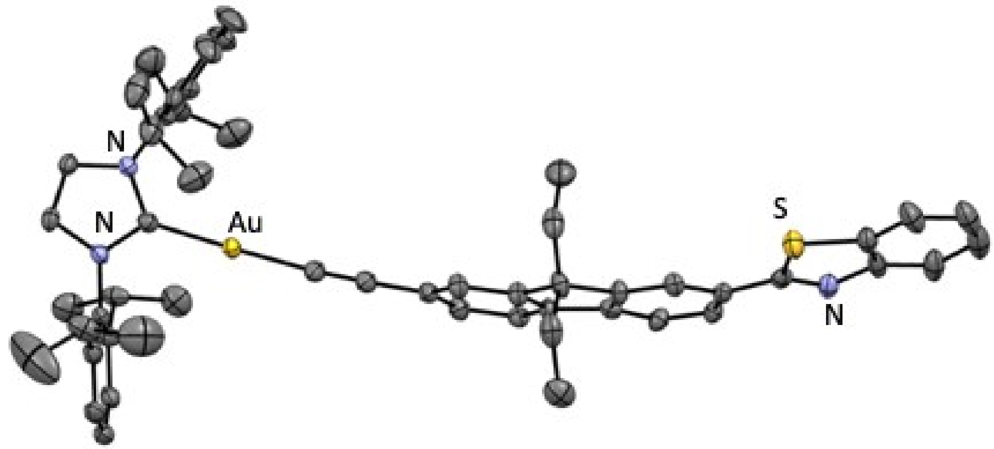

Figure S2. Thermal ellipsoid representation of **Au-ABTF2** (50% probability level, 150 K). Hydrogen atoms are omitted for clarity. Unlabeled atoms are carbon.

ABTF1:

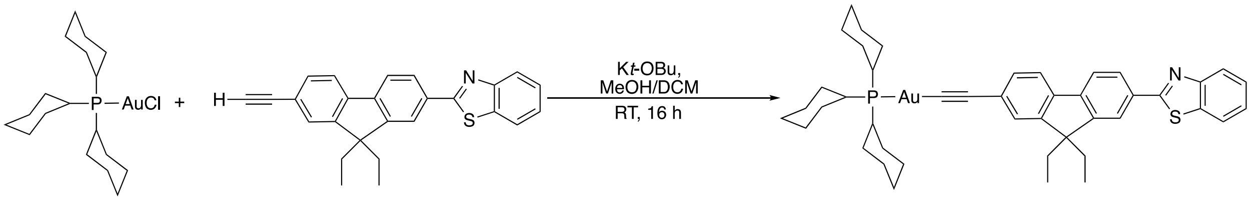

Prep: To a 20 mL scintillation vial equipped with a stir bar was added (24.1 mg, 0.215 mmol) of potassium *tert*-butoxide along with 4 mL of MeOH via syringe. The suspension was stirred until a solution was observed, after which (81.5 mg, 0.215 mmol) of BTF alkyne was added. Most didn't dissolve, so 3 mL of DCM was added creating a yellow solution. This solution was stirred at RT for 45 min and then transferred to another 20 mL scint. vial containing 2 mL of MeOH and (100 mg, 0.195 mmol) Cy_3PAuCl, creating a yellow/brown solution. This solution was stirred in the absence of light for 16 h and then concentrated *in vacuo*. The brown/yellow solid was dissolved in dichloromethane, filtered over Celite, concentrated, and washed with (4 x 25 mL) of pentanes. The brown solid was allowed to dry and then subjected to crystallization via slow diffusion of pentanes into a concentrated dichloromethane solution yielding 100 mg of analytically pure material. (Yield 60 %). ^{1}H NMR (500 MHz, Chloroform-*d*) δ 8.10 – 8.05 (m, 2H), 8.00 (dd, *J* = 7.9, 1.7 Hz, 1H), 7.91 (d, *J* = 8.0 Hz, 1H), 7.73 (d, *J* = 7.9 Hz, 1H), 7.62 (d, *J* = 7.8 Hz, 1H), 7.55 – 7.45 (m, 3H), 7.40 – 7.35 (m, 1H), 2.18 – 1.96 (m, 13H), 1.86 (d, *J* = 11.0 Hz, 7H), 1.75 (s, 2H), 1.50 (d, *J* = 12.7 Hz, 7H), 1.29 (t, *J* = 11.7 Hz, 9H), 0.30 (t, *J* = 7.3 Hz, 6H).^{31}P NMR (121 MHz, CDCl$_3$) δ (ppm): 56.41. HRMS (FT-ICR, [M+H]$^{+}$) m/z calcd for MH^{+}C$_{44}$H$_{54}$AuNPS^{+}856.33746, found 856.33733. Anal. Calcd for: C$_{44}$H$_{53}$AuNPS: C, (61.74); H, (6.24); N, (1.64). Found: C, (61.48); H, (6.07); N, (1.79).

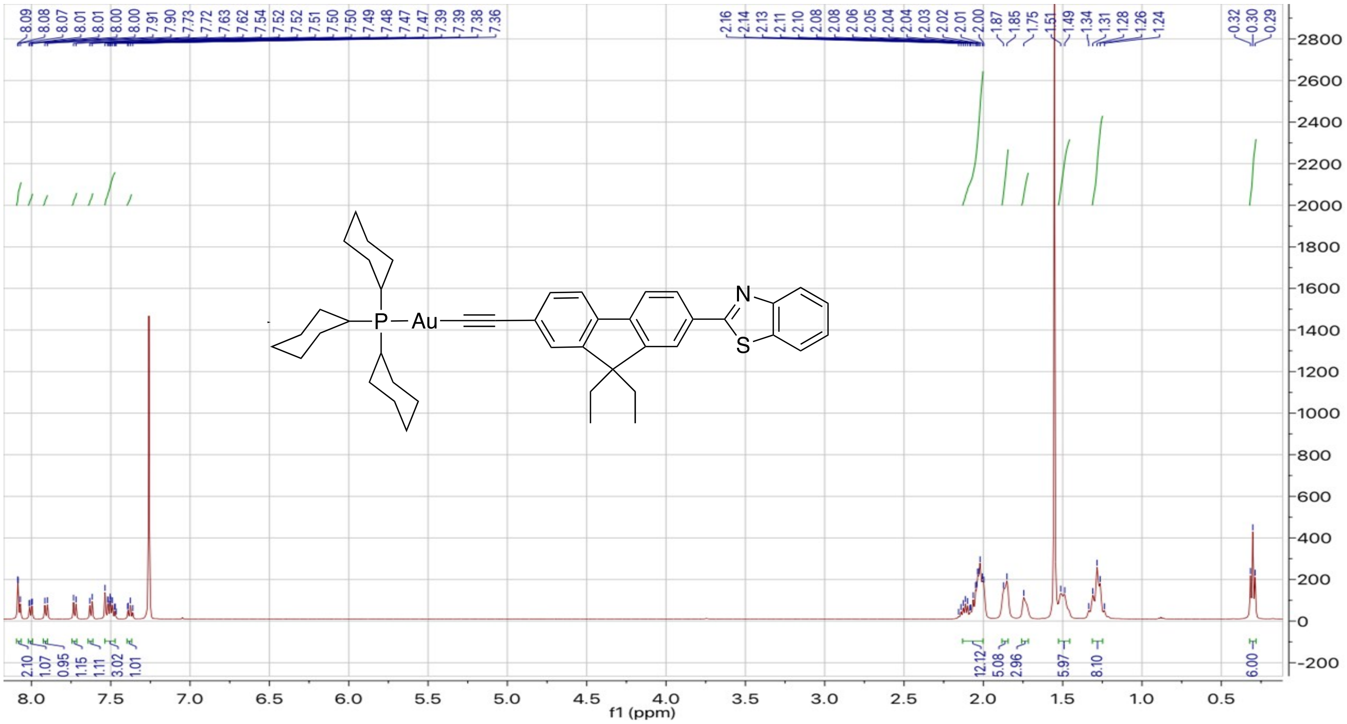

Figure S3. ^{1}H NMR of **Au-ABTF1**

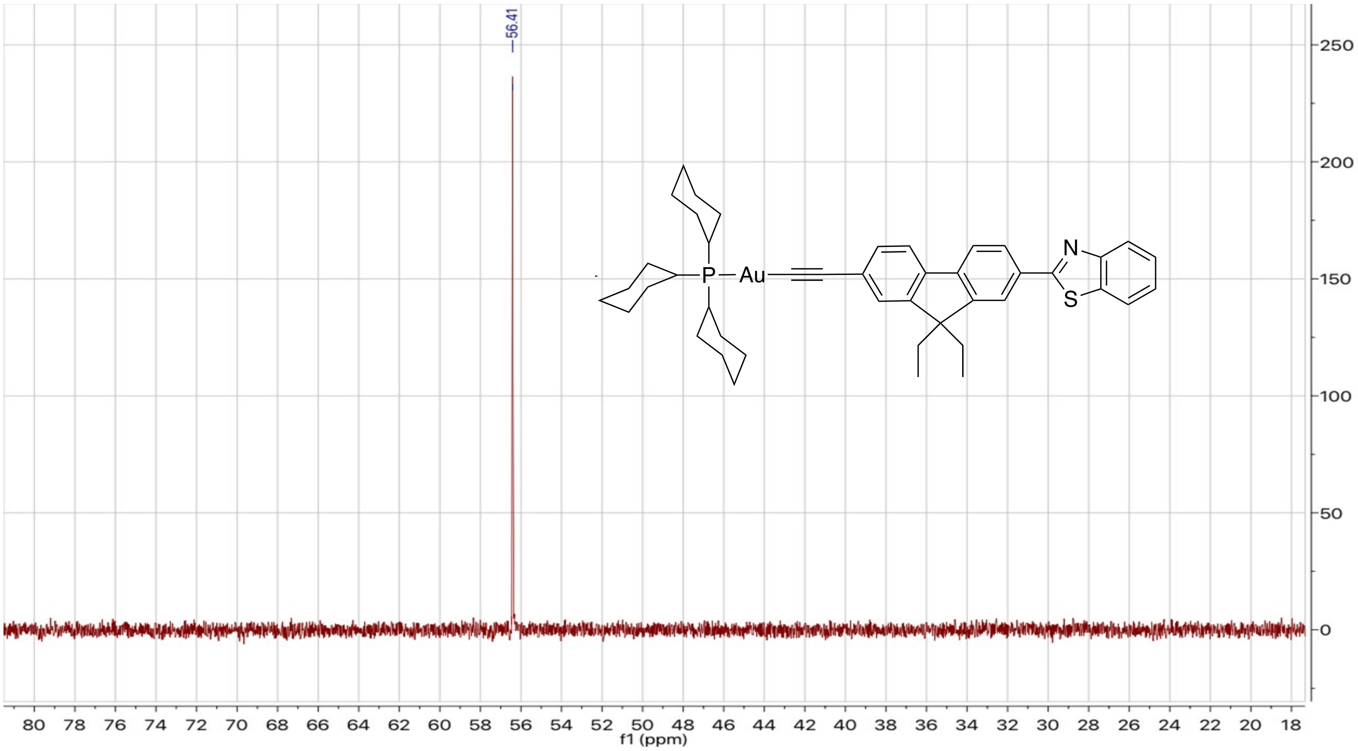

Figure S4. ^{31}P NMR of **Au-ABTF1**

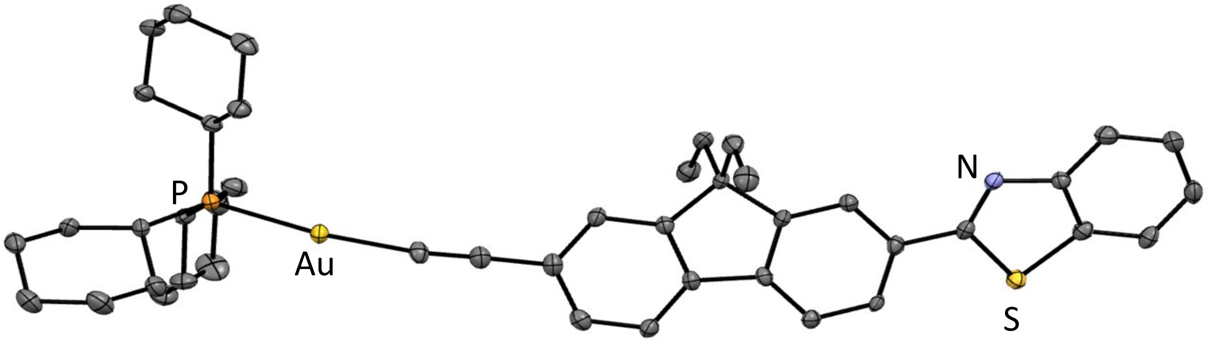

Figure S5. Thermal ellipsoid representation of **Au-ABTF1** (50% probability level, 150 K). Hydrogen atoms are omitted for clarity. Unlabeled atoms are carbon.

Au-ABTF0:

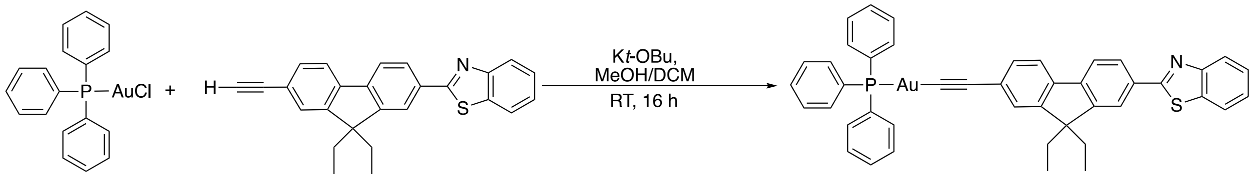

Prep: To a 20 mL scintillation vial equipped with a stir bar was added (29.5 mg, 0.263 mmol) of potassium *tert*-butoxide along with 4 mL of MeOH via syringe. The suspension was stirred until a solution was observed, after which (99.6 mg, 0.263 mmol) of BTF alkyne was added. Most didn't dissolve, so 3 mL of DCM was added creating a yellow solution. This solution was stirred at RT for 45 min and then transferred to another 20 mL scint. vial containing 2 mL of MeOH and (100 mg, 0.202 mmol) Ph$_3$AuCl, creating a yellow/brown solution. This solution was stirred in the absence of light for 16 h and then concentrated *in vacuo*. The brown/yellow solid was dissolved in dichloromethane, filtered over Celite, concentrated, and washed with (4 x 25 mL) of pentanes. The brown solid was allowed to dry and then subjected to crystallization via slow diffusion of pentanes into a concentrated dichloromethane solution yielding 135 mg of analytically pure material. (Yield 79 %). ^{1}H NMR (500 MHz, Chloroform-*d*) δ 8.11 – 8.06 (m, 2H), 8.01 (dd, *J* = 7.9, 1.7 Hz, 1H), 7.91 (d, *J* = 7.8 Hz, 1H), 7.74 (d, *J* = 7.9 Hz, 1H), 7.65 (d, *J* = 7.8 Hz, 1H), 7.62 – 7.43 (m, 18H), 7.42 – 7.35 (m, 1H), 2.09 (m, *J* = 28.5, 7.0 Hz, 4H), 0.32 (t, *J* = 7.3 Hz, 6H). ^{31}P NMR (121 MHz, CDCl$_3$) δ (ppm): 42.35. HRMS (FT-ICR, $[M+H]^+$) m/z calcd for $MH^+C_{44}H_{36}AuNPS^+$, 838.19661 found 838.19670. Anal. Calcd for: $C_{44}H_{35}AuNPS$: C, (63.08); H, (4.21); N, (1.67). Found: C, (62.97); H, (4.25); N, (1.72).

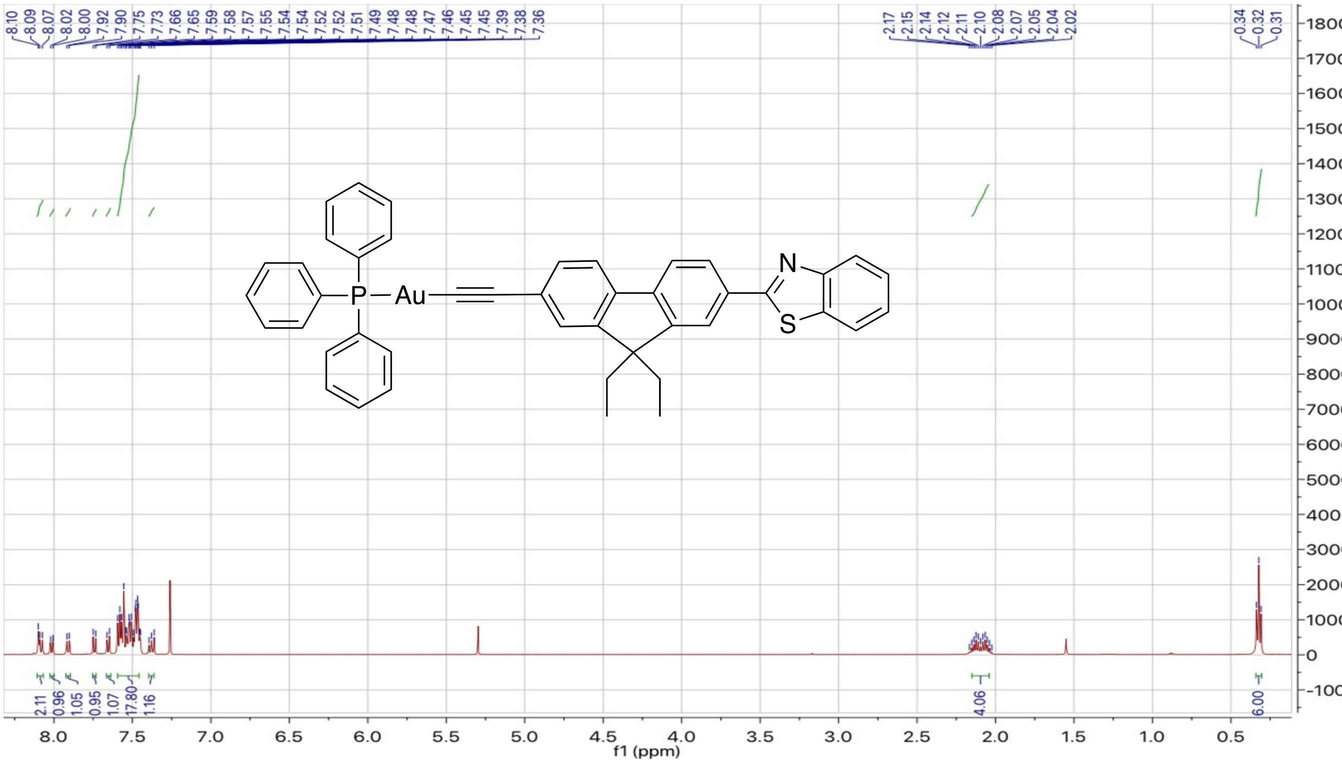

Figure S6. ^{1}H NMR of **Au-ABTF0**

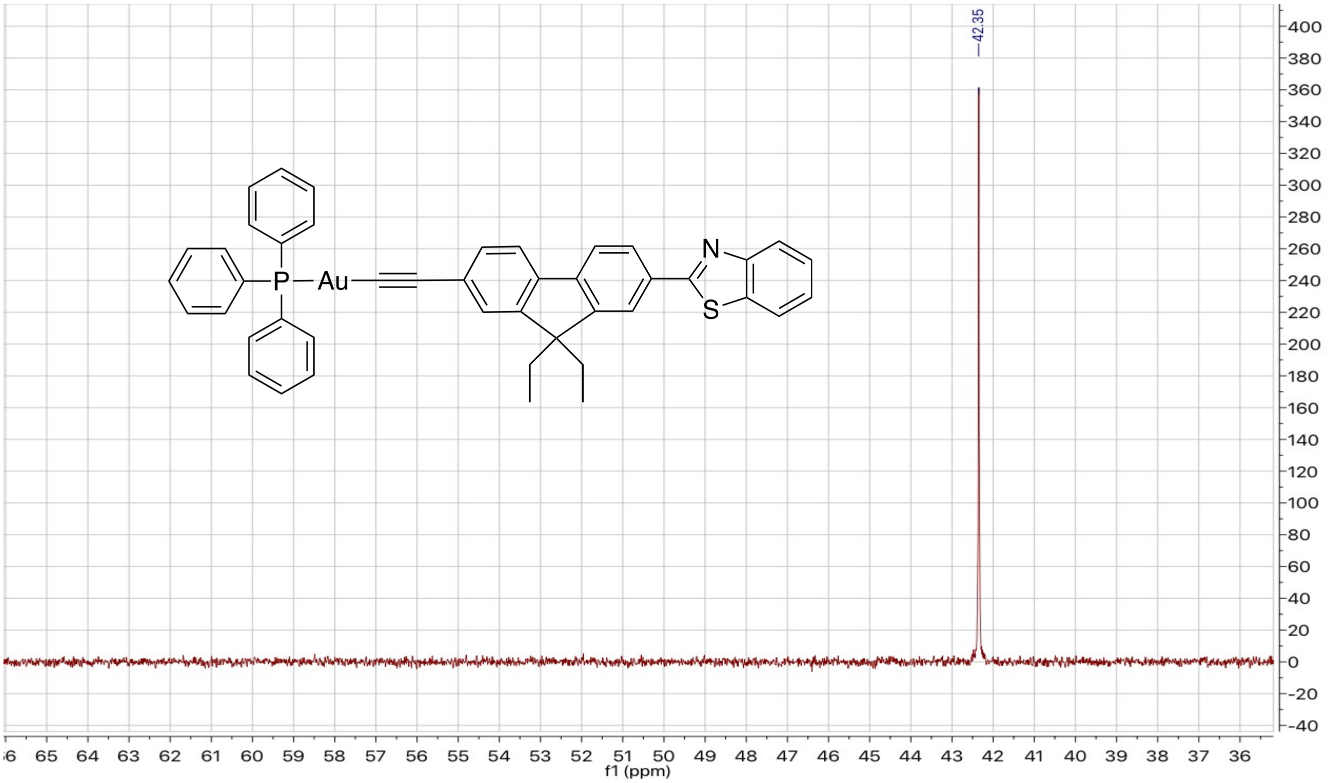

Figure S7. ^{31}P NMR of **Au-ABTF0**

Crystal Stucutre of $Ph_3PAuBTF$ alkyne

Figure S8. Thermal ellipsoid representation of **Au-ABTF0** (50% probability level, 150 K). Hydrogen atoms are omitted for clarity. Unlabeled atoms are carbon.

III. Supplemental Figures

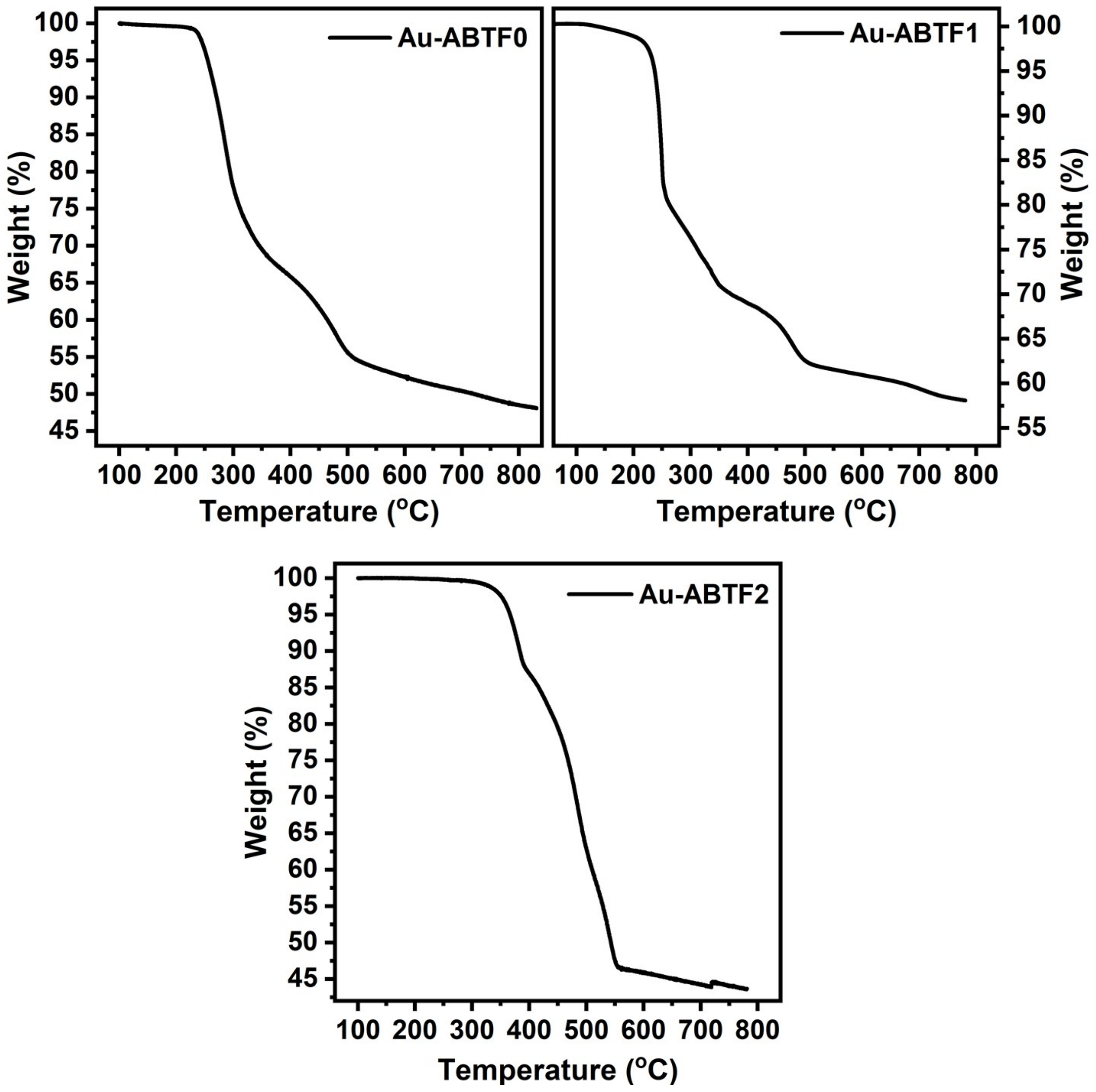

Figure S9: Thermogravimetric Analysis of Au-ABTF0 (top left), Au-ABTF1 (top right), Au-ABTF2 (bottom center).

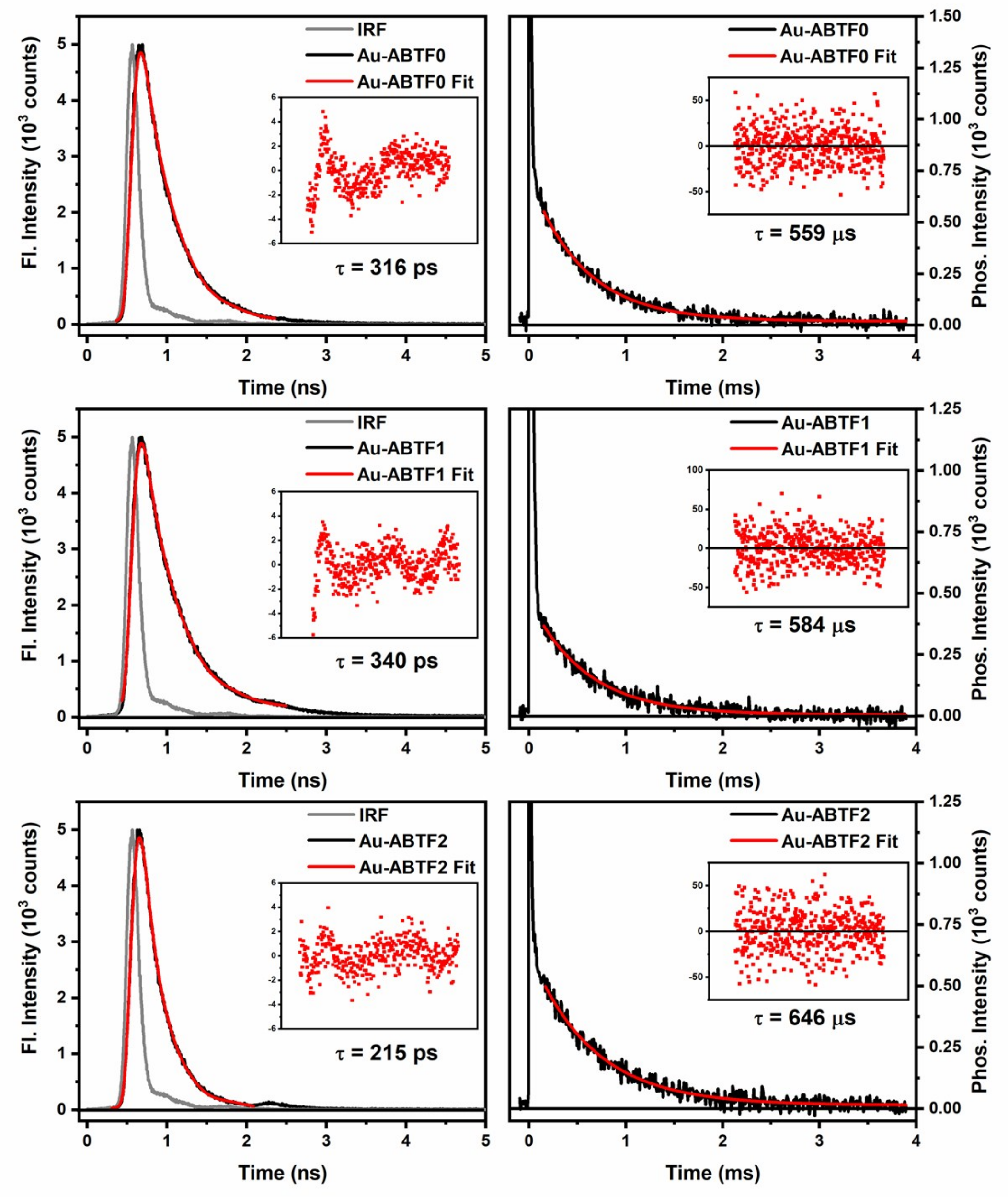

Figure S10: Fluorescence Lifetimes with IRF (Left) and Phosphorescence Lifetimes (Right) of Au-ABTF0 (Top), Au-ABTF1 (Middle), and Au-ABTF2 (Bottom). *All lifetime values were collected in toluene. The fluorescence lifetimes were fit using the reconvolution fit provided by Edinburgh Instruments. The phosphorescence lifetimes were obtained following three freeze-pump-thaw degas cycles and fit using a monoexponential decay equation in Origin. Residuals for all fits are provided in the inset. Table 2 summarizes the lifetime averages of duplicate trials.*

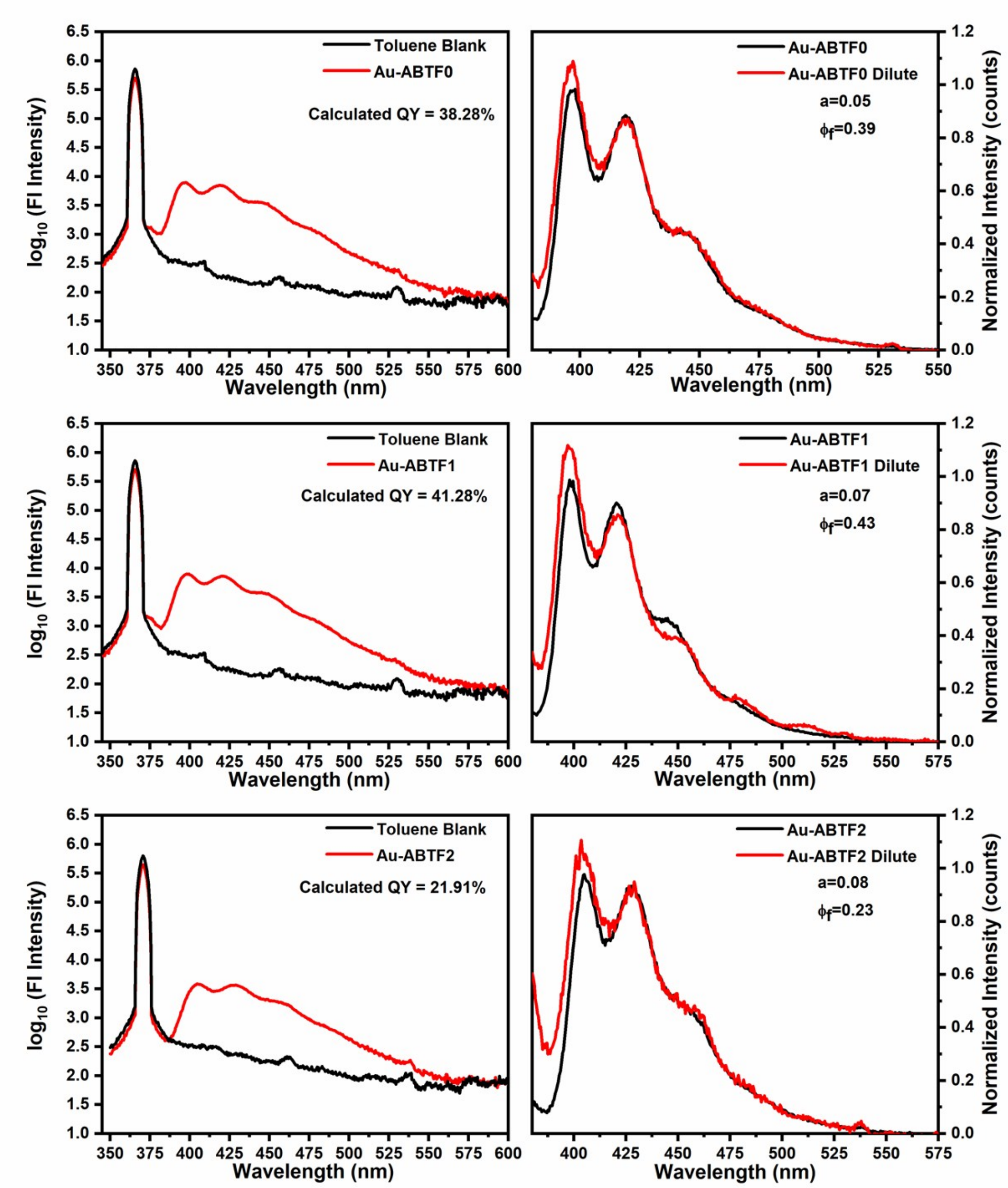

Figure S11: Raw (Left) and Corrected (Right) Fluorescence Quantum Yields of Au-ABTF0 (Top), Au-ABTF1 (Middle), and Au-ABTF2 (Bottom). *Fluorescence quantum yield values were collected in toluene. The dilute samples used for the reabsorption correction were a one tenth serial dilution of the concentrated samples. The experiments were performed in duplicate with the average value reported in Table 2.*

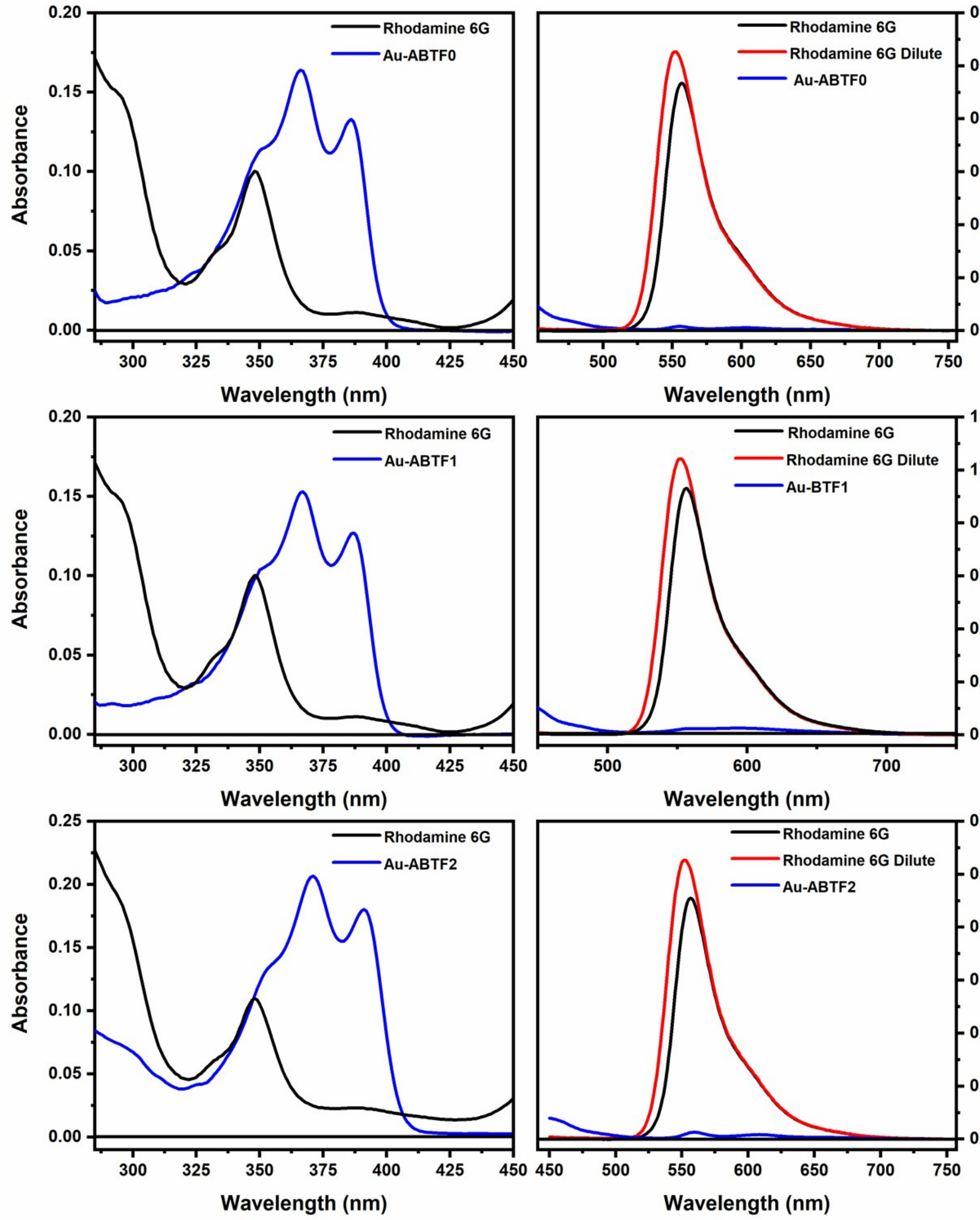

Figure S12: Ground State Absorption (Left) and Luminescence Emission (Right) of reference Rhodamine 6G and Au-ABTF0 (Top), Au-ABTF1 (Middle), and Au-ABTF2 (Bottom) for Phosphorescence Quantum Yields. *Au-ABTF samples were collected in toluene and Rhodamine 6G was collected in ethanol. All experiments were performed in duplicate with average values reported in Table 2.*

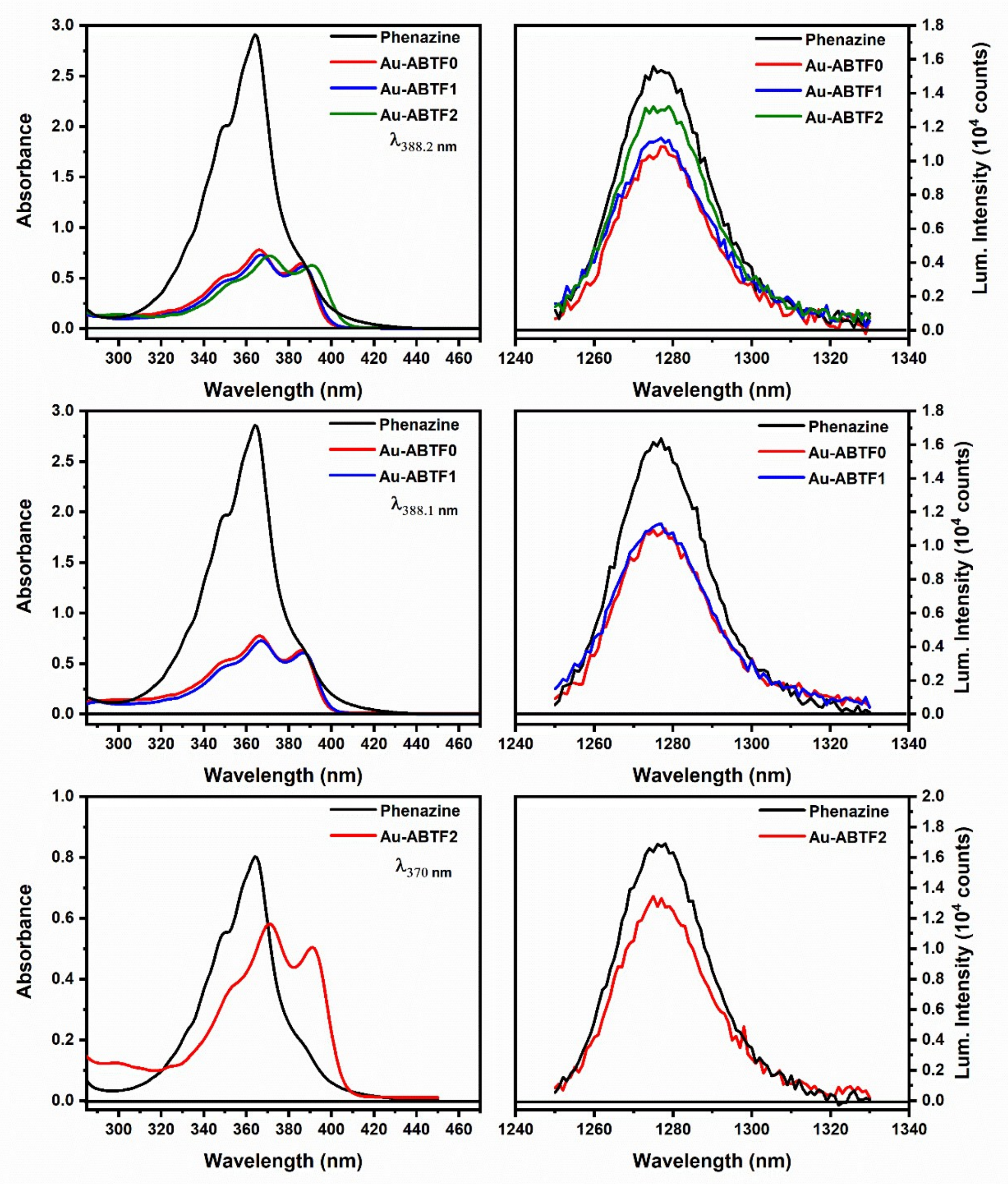

Figure S13: Ground State Absorption (Left) and Singlet Oxygen Emission (Right). *The top figures portray trial one of all samples, the middle figures portray trial two of Au-ABTF0 and Au-ABTF1, and the bottom figures portray trial two of Au-ABTF2. All experiments were performed in toluene using phenazine as a reference. The average triplet quantum yield is reported in Table 2.*

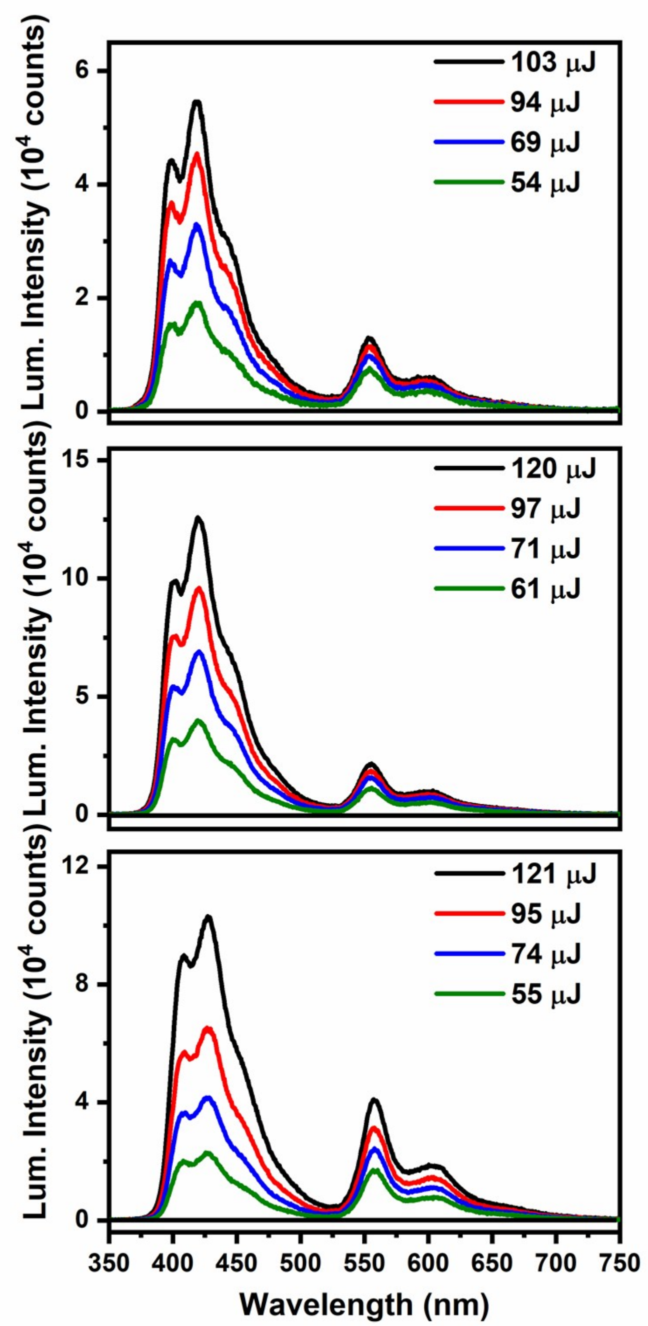

Figure S14: Delayed Fluorescence of Au-ABTF0 (Top), Au-ABTF1 (Middle), and Au-ABTF2 (Bottom). *The experiments were performed in freeze-pump-thaw degassed toluene solutions. Spectra were collected using 355 nm excitation, a 50 µs bandwidth, and a 99 µs gate width on the Andor iStar ICCD camera.*

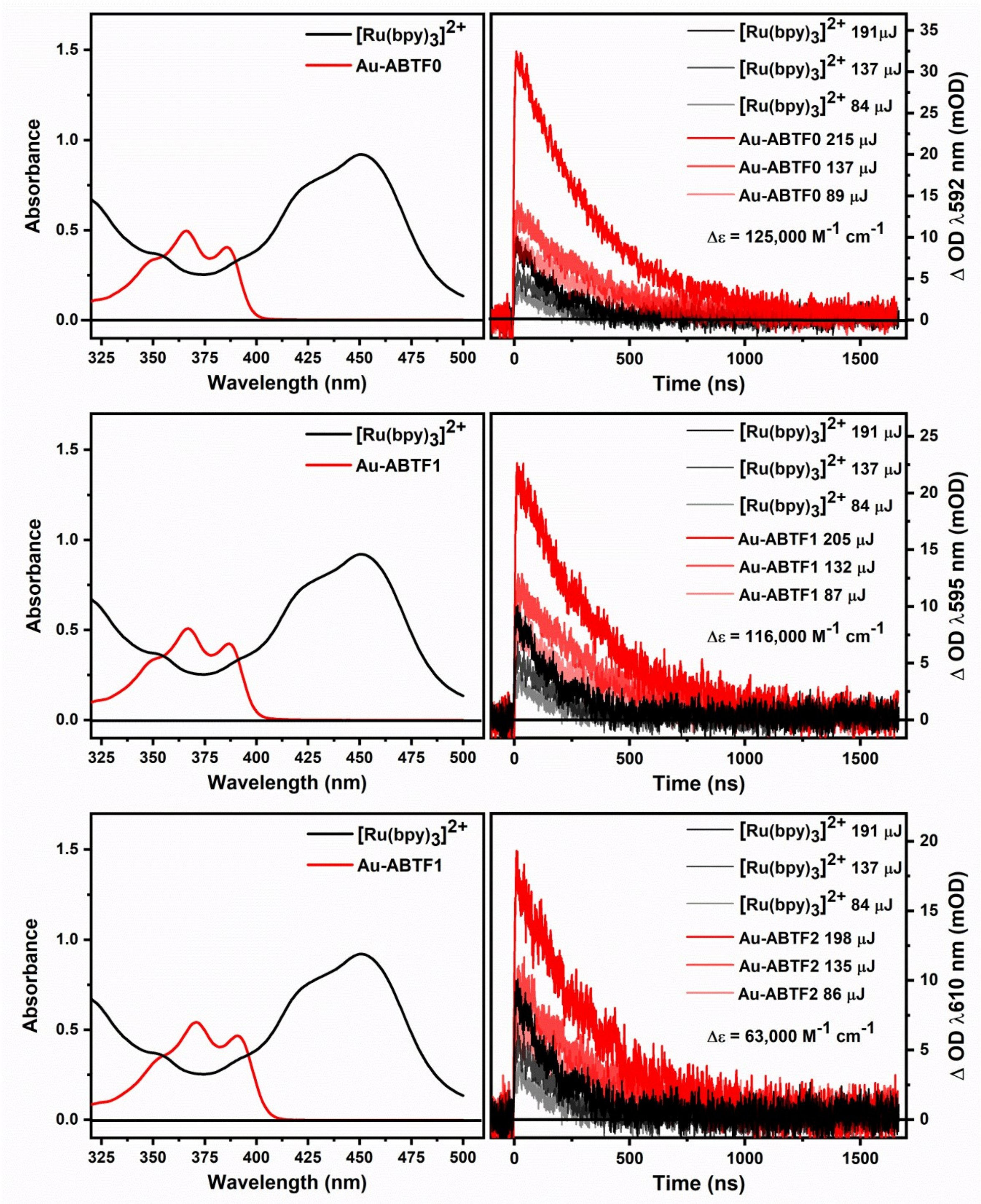

Figure S15: Ground State Absorption (Left) and Excited State Decay Traces at Three Laser Excitation Energies of Au-ABTF0 (Top), Au-ABTF1 (Middle), and Au-ABTF2 (Bottom) in Toluene. *$[Ru(bpy)_3]^{2+}$ dissolved in acetonitrile was used as the actinometer. 370 nm was used as the detection wavelength for $[Ru(bpy)_3]^{2+}$ samples. Au-ABTF data was collected in toluene and the transient absorption signal was monitored at the maximum of the triplet-triplet absorption in each sample. All experiments were performed in aerated solutions with 355* *nm excitation and fit to monoexponential fits in Origin. The average of two trials is reported in* Table 1.

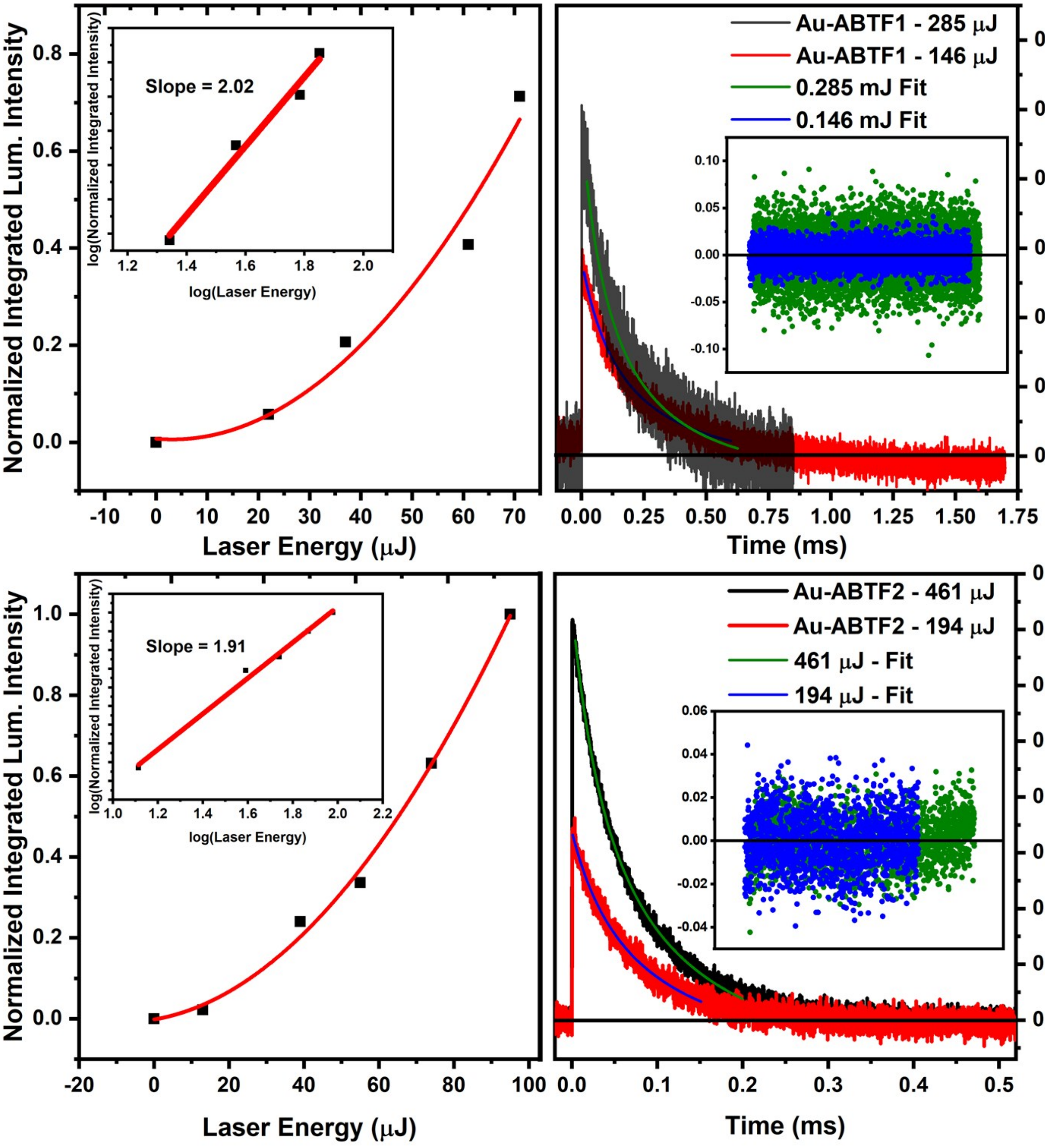

Figure S16: Fits of the Normalized Integrated Fluorescence Intensity vs. Laser Pulse Energy (Left) and Triplet Triplet Annihilation Fitting of Excited-State Decay Traces of Au-ABTF1 (Top) and Au-ABTF2 (Bottom). *Experiments were performed in freeze-pump-thaw deaerated solutions. The insets represent the double logarithm plot (Left) and residuals of the fit data (Right). Au-ABTF1 285 μJ kinetic data is shown at 25% transparency for clarity.*

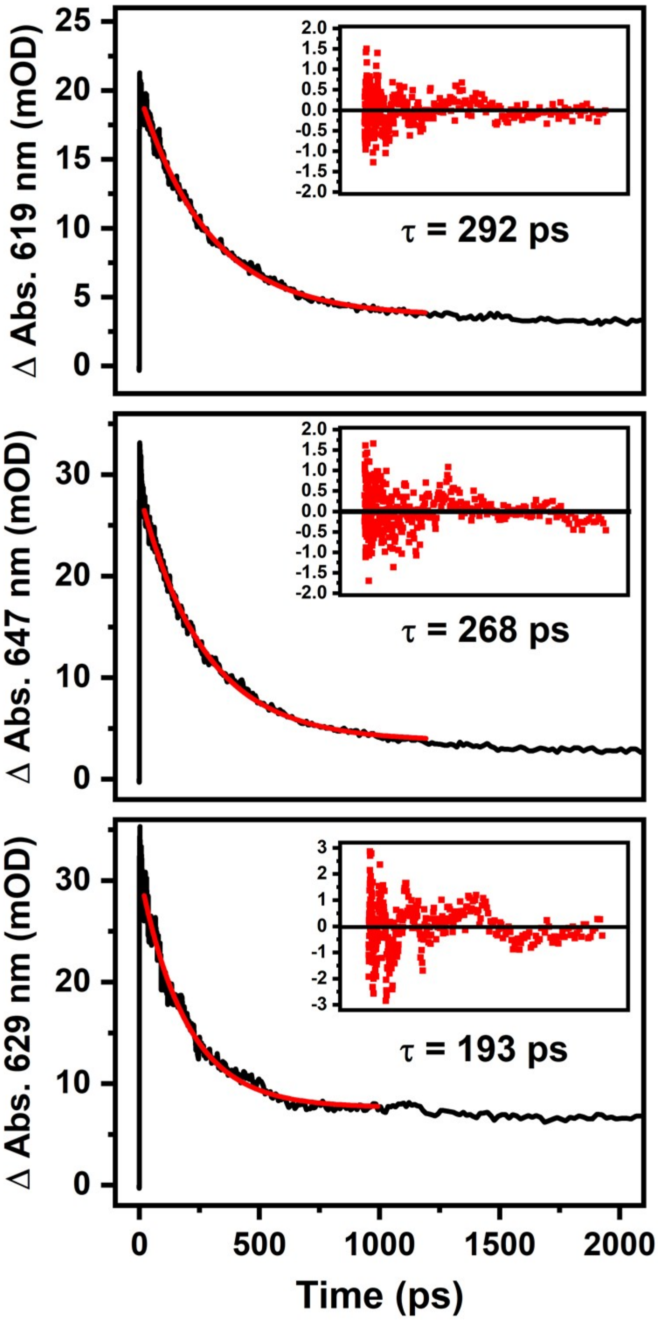

Figure S17: Ultrafast Transient Absorption Decay Trace for Au-ABTF0 (Top), Au-ABTF1 (Middle), and Au-ABTF2 (Bottom) in Aerated Toluene. *Lifetime values were collected in aerated toluene. Residuals of the fits are portrayed in the insets. Lifetimes reported in the figure* *represent the fit obtained from a single wavelength. The average lifetime value obtained from fits at ten wavelengths in the TA spectra is reported in Table 3.*

Table S1: Phosphorescence Lifetimes Final Cell Pressures. *All trials were deaerated using freeze-pump-thaw methods in toluene.*

Complex	Final Cell Pressure (mTorr)	
	Trial 1	Trial 2
Au-ABTF0	95	95
Au-ABTF1	85	85
Au-ABTF2	92	92

IV. X-Ray Crystallography

Single crystals of **Au-ABTF0**, **Au-ABTF1** and **Au-ABTF2** were selected under a stereomicroscope with polarizing filter and mounted with the aid of a trace of Fomblin oil on the goniometer head of a Bruker Quest diffractometer with a fixed chi angle, a sealed tube fine focus X-ray tube, single crystal curved graphite incident beam monochromator, a Photon100 CMOS area detector and an Oxford Cryosystems low temperature device. Examination and data collection were performed with Mo Kα radiation (λ = 0.71073 Å) at 150 K. Data were collected, reflections were indexed and processed, and the files scaled and corrected for absorption using APEX3. The space groups were assigned and the structures were solved by direct methods using XPREP within the SHELXTL suite of programs[12] and refined by full matrix least squares against F^2 with all reflections using Shelxl2018[13] using the graphical interface Shelxle.[14] If not specified otherwise H atoms attached to carbon atoms were positioned geometrically and constrained to ride on their parent atoms. C-H bond distances were constrained to 0.95 Å for aromatic moieties, and to 1.00, 0.99 and 0.98 Å for aliphatic C-H, CH_2 and CH_3 moieties, respectively. Methyl CH_3 H atoms were allowed to rotate but not to tip to best fit the experimental electron density. $U_{iso}(H)$ values were set to a multiple of $U_{eq}(C)$ with 1.5 for CH_3, NH_3^+ and OH, and 1.2 for C-H, CH_2, B-H, N-H and NH_2 units, respectively.

In Au-ABTF2, a solvate methylene chloride molecule was refined as partially occupied. The occupancy rate refined to 0.784(5).

Additional refinement details are given in the table, below.

Complete crystallographic data, in CIF format, have been deposited with the Cambridge Crystallographic Data Centre. CCDC 1953520-1953522 contains the supplementary crystallographic data for this paper. These data can be obtained free of charge from The Cambridge Crystallographic Data Centre via www.ccdc.cam.ac.uk/data_request/cif.

Table S2. Experimental details

	jjm_1_141_0m	jjm_1_145_0m	jjm_1_139_0m
Crystal data			
Chemical formula	$C_{44}H_{35}AuNPS$	$C_{44}H_{53}AuNPS$	$C_{53}H_{56}AuN_3S\cdot0.784(CH_2Cl_2)$
M_r	837.72	855.87	1030.59
Temperature (K)	150	150	150
Crystal system, space group	Triclinic, $P\bar{1}$	Triclinic, $P\bar{1}$	Orthorhombic, $P2_12_12_1$
a, b, c (Å)	8.7524 (4), 13.6920 (6), 16.4993 (8)	10.5754 (5), 14.0285 (7), 14.1291 (9)	15.0586 (5), 17.6860 (7), 19.2675 (8)
α, β, γ (°)	114.3972 (15), 90.4473 (18), 103.7777 (16)	106.091 (2), 98.004 (2), 106.3596 (17)	90, 90, 90
V (Å^3)	1736.22 (14)	1878.03 (18)	5131.4 (3)
Z	2	2	4
Radiation type	Mo $K\alpha$	Mo $K\alpha$	Mo $K\alpha$
F(000)	832	868	2092
D_x (Mg m^{-3})	1.602	1.514	1.334
No. of reflections for cell measurement	9797	7259	9988
θ range (°) for cell measurement	3.1–30.6	2.9–28.3	2.9–32.0
μ (mm^{-1})	4.38	4.05	3.03
Crystal shape	Block	Plate	Block
Colour	Colourless	Colourless	Colourless
Crystal size (mm)	0.24 × 0.17 × 0.16	0.09 × 0.08 × 0.02	0.21 × 0.17 × 0.11
Data collection			
Diffractometer	Bruker AXS D8 Quest CMOS diffractometer		
Radiation source	sealed tube X-ray source		
Monochromator	Triumph curved graphite crystal		
Scan method	ω and phi scans		
Absorption correction	Multi-scan, SADABS 2016/2[15]		
Radiation source	sealed tube X-ray source		
T_{min}, T_{max}	0.650, 0.747	0.632, 0.746	0.647, 0.747
No. of measured, independent and	51677, 13091, 10286	26102, 8750, 7004	54147, 15987, 11944

observed [$I > 2\sigma(I)$] reflections			
R_{int}	0.040	0.079	0.044
θ values (°)	$\theta_{\max} = 33.2$, $\theta_{\min} = 3.3$	$\theta_{\max} = 28.3$, $\theta_{\min} = 3.0$	$\theta_{\max} = 33.2$, $\theta_{\min} = 2.9$
$(\sin \theta/\lambda)_{\max}$ (Å^{-1})	0.771	0.667	0.770
Range of h, k, l	$h = -13\rightarrow13$, $k = -20\rightarrow20$, $l = -25\rightarrow25$	$h = -14\rightarrow14$, $k = -18\rightarrow18$, $l = -18\rightarrow18$	$h = -18\rightarrow20$, $k = -20\rightarrow25$, $l = -24\rightarrow29$
Refinement			
Refinement on	F^2		
$R[F^2 > 2\sigma(F^2)]$, $wR(F^2)$, S	0.032, 0.058, 1.01	0.034, 0.074, 1.04	0.032, 0.057, 0.95
No. of reflections	13091	8750	15987
No. of parameters	435	435	561
No. of restraints	0		
H-atom treatment	H-atom parameters constrained		
Weighting scheme	$w = 1/[\sigma^2(F_o^2) + (0.0192P)^2 + 1.2299P]$ where $P = (F_o^2 + 2F_c^2)/3$	$w = 1/[\sigma^2(F_o^2) + (0.0242P)^2 + 0.4044P]$ where $P = (F_o^2 + 2F_c^2)/3$	$w = 1/[\sigma^2(F_o^2) + (0.0111P)^2]$ where $P = (F_o^2 + 2F_c^2)/3$
$(\Delta/\sigma)_{\max}$	0.003	0.001	0.003
$\Delta\rho_{\max}$, $\Delta\rho_{\min}$ (e Å^{-3})	2.40, -1.58	1.95, -0.99	2.05, -0.93
Absolute structure	–	–	Flack x determined using 4436 quotients [(I+)-(I-)]/[(I+)+(I-)][16]
Absolute structure parameter	–	–	-0.013 (3)

Computer programs: Apex3 v2016.9-0 (Bruker, 2016), *SAINT* V8.37A (Bruker, 2016), *SHELXS97*[12], *SHELXL2018*/3[13], SHELXLE Rev900[14].

V. Calculations

Spin-restricted and time-dependent density-functional theory computations proceeded in Gaussian16 rev. A.03.[17] Geometries were optimized with the 6-31G(d) basis set for nonmetal atoms and the Stuttgard-Dresden effective core potential and basis set for Au.[18] Optimizations proceeded without constraints, and harmonic frequency calculations found all real vibrational frequencies, confirming that converged structures are local energy minima. Final single-point calculations employed the exchange and correlation functionals of Perdew, Burke, and Ernzerhof (PBE0),[19] and the TZVP basis set of Godbelt, Andzelm, and co-workers for nonmetals.[20] For metal atoms, the Stuttgart-Dresden effective core potential and basis set were used; scalar relativistic effects are included implicitly. Continuum solvation in toluene was imposed using the integral equation formalism of the polarizable continuum model.[21–24] Population analyses were performed with the AOMix-CDA program of Gorelsky.[25,26]

Table S3. AuABTF0: Summary of calculated electronic transitions to Franck-Condon <u>singlet</u> states.

HOMO = 178; LUMO = 179

```
  #    nm  1000 cm-1   eV     f     Assignment (excitations with contrib. greater than 10.0%)
  1  392.8   25.46   3.156  1.9462  178->179(97.5%)
  2  316.5   31.59   3.917  0.0003  178->181(94.2%)
  3  315.6   31.68   3.928  0.0287  178->180(93.5%)
  4  302.4   33.07   4.100  0.0001  176->179(81.8%) 176->183(11.3%)
  5  301.1   33.21   4.118  0.0840  177->179(80.8%) 175->179(12.3%)
  6  297.6   33.60   4.166  0.0256  175->179(37.2%) 178->186(14.3%) 177->179(13.1%) 178-
>183(11.3%)
  7  294.1   34.00   4.216  0.0435  175->179(38.7%) 178->183(21.8%) 178->186(11.8%)
  8  290.7   34.40   4.265  0.0001  178->182(97.3%)
  9  287.5   34.78   4.313  0.1121  178->183(46.3%) 174->179(21.0%) 178->187(11.0%)
 10  281.4   35.54   4.406  0.0813  174->179(45.4%) 172->179(17.9%) 178->183(11.2%)
 11  276.9   36.11   4.478  0.0002  178->184(97.2%)
 12  275.4   36.31   4.502  0.0001  178->185(74.7%) 178->189(15.3%)
 13  264.1   37.87   4.695  0.0470  172->179(46.4%) 178->186(36.9%)
 14  262.0   38.17   4.732  0.0134  178->187(66.4%) 178->186(18.1%)
 15  256.7   38.95   4.829  0.0024  176->180(44.6%) 164->179(42.8%)
 16  256.4   39.00   4.835  0.0014  164->179(47.9%) 176->180(39.7%)
 17  256.0   39.06   4.843  0.0102  178->188(64.2%)
 18  255.5   39.13   4.852  0.0722  176->181(63.8%) 178->188(11.1%)
 19  253.6   39.43   4.888  0.0647  173->179(72.2%) 173->180(19.8%)
 20  253.5   39.44   4.891  0.0001  178->189(56.6%) 178->185(20.6%) 177->181(14.0%)
 21  249.5   40.08   4.969  0.0811  177->180(75.0%) 176->181(14.2%)
 22  247.6   40.38   5.006  0.0181  177->181(71.9%) 178->189(14.6%)
 23  246.8   40.53   5.025  0.1286  173->181(83.5%)
 24  245.0   40.81   5.060  0.0227  171->179(81.9%)
 25  244.3   40.93   5.074  0.0404  178->190(30.1%) 178->191(25.7%) 173->180(12.6%)
 26  244.1   40.97   5.079  0.1327  173->180(57.8%) 173->179(14.3%)
 27  241.4   41.42   5.135  0.0096  173->182(30.6%) 169->180(15.8%) 168->181(15.1%)
```

```
 28  240.9   41.51   5.147  0.0166  178->190(25.1%) 178->191(24.7%) 177->183(12.7%)
 29  239.8   41.70   5.170  0.0001  176->183(67.2%)
 30  238.3   41.96   5.202  0.0006  176->182(91.8%)
 31  235.6   42.44   5.262  0.0158  175->180(65.7%) 175->183(11.8%)
 32  235.5   42.46   5.264  0.0086  170->179(69.4%) 170->180(11.4%)
 33  234.7   42.61   5.282  0.0023  177->182(23.4%) 168->181(10.2%)
 34  234.6   42.62   5.284  0.0418  177->183(57.0%) 178->190(13.1%)
 35  234.2   42.70   5.294  0.0130  168->180(12.7%) 173->185(12.5%) 169->181(12.1%) 167-
>181(11.5%)
 36  233.5   42.83   5.310  0.0015  177->182(68.7%)
 37  233.2   42.88   5.317  0.0000  175->181(98.9%)
 38  232.2   43.07   5.340  0.0002  178->193(72.7%) 177->193(12.1%)
 39  231.5   43.21   5.357  0.0045  178->192(77.6%)
 40  230.1   43.46   5.388  0.0116  175->180(19.5%) 177->187(16.9%) 175->183(16.0%) 177-
>186(12.3%)
```

Table S4. AuABTF0: Summary of calculated electronic transitions to Franck-Condon triplet states.

HOMO = 178; LUMO = 179

```
  #    nm  1000 cm-1   eV     f     Assignment (excitations with contrib. greater than 10.0%)
  1  559.9   17.86   2.214  0.0000  178->179(78.6%)
  2  430.4   23.24   2.881  0.0000  177->179(46.0%) 178->183(23.0%)
  3  363.8   27.49   3.408  0.0000  175->179(38.3%)
  4  353.4   28.30   3.509  0.0000  173->180(18.4%) 169->182(11.3%)
  5  353.3   28.30   3.509  0.0000  173->181(19.2%) 168->182(11.1%)
  6  352.1   28.40   3.522  0.0000  166->181(13.3%) 165->180(11.3%) 167->182(10.4%)
  7  332.5   30.08   3.729  0.0000  175->179(25.8%) 178->186(16.4%) 171->179(10.1%)
  8  327.5   30.54   3.786  0.0000  178->187(19.5%) 178->186(13.0%)
  9  325.8   30.70   3.806  0.0000  172->179(28.7%) 177->179(13.2%) 178->180(12.3%)
 10  320.1   31.24   3.873  0.0000  178->181(62.9%) 176->179(17.4%)
```

Table S5. AuABTF1: Summary of calculated electronic transitions to Franck-Condon singlet states.

HOMO = 187; LUMO = 188

```
  #    nm  1000 cm-1   eV     f     Assignment (excitations with contrib. greater than 10.0%)
  1  395.1   25.31   3.138  1.8708  187->188(97.5%)
  2  306.8   32.59   4.041  0.0000  185->188(83.4%) 185->189(13.4%)
  3  302.3   33.08   4.102  0.1135  186->188(86.2%)
  4  298.9   33.46   4.149  0.0260  187->189(41.6%) 187->190(23.3%) 184->188(12.1%) 181-
>188(10.4%)
  5  294.9   33.91   4.205  0.1009  184->188(65.1%) 187->189(20.5%)
  6  290.4   34.43   4.269  0.1285  187->190(37.5%) 187->189(26.9%) 183->188(16.5%)
  7  281.7   35.49   4.401  0.0713  183->188(50.7%) 181->188(18.5%) 187->195(11.7%)
  8  275.8   36.26   4.496  0.0039  187->192(82.8%)
  9  264.6   37.79   4.685  0.0317  181->188(51.6%) 187->190(26.1%) 183->188(13.5%)
 10  257.8   38.80   4.810  0.0040  187->191(70.8%)
 11  256.3   39.01   4.837  0.0004  178->188(91.8%)
 12  253.0   39.52   4.900  0.0140  182->188(92.9%)
 13  248.9   40.17   4.981  0.0221  187->193(67.3%)
 14  248.1   40.31   4.998  0.0021  185->189(63.5%) 185->188(14.2%)
 15  246.2   40.63   5.037  0.0194  180->188(85.1%)
 16  244.9   40.83   5.062  0.0849  187->195(64.0%)
 17  239.6   41.74   5.175  0.0056  187->194(85.4%)
 18  237.1   42.18   5.230  0.0364  186->189(65.4%) 187->193(11.6%)
 19  233.2   42.89   5.318  0.0001  187->196(82.5%) 186->196(13.5%)
 20  232.3   43.06   5.338  0.0465  184->189(34.5%) 186->190(24.2%) 186->191(12.5%)
 21  228.9   43.68   5.415  0.0061  186->190(39.6%) 185->192(14.5%)
 22  228.6   43.75   5.425  0.0008  185->190(62.7%) 185->195(10.8%)
 23  226.0   44.24   5.485  0.3480  185->192(26.2%) 184->189(17.5%) 186->190(17.3%) 187-
>197(10.2%)
 24  225.4   44.37   5.501  0.0009  179->188(92.6%)
 25  223.3   44.77   5.551  0.3159  187->197(39.5%) 185->192(26.3%)
```

```
 26  219.0   45.66   5.662  0.2439  183->189(38.1%) 187->197(11.2%) 184->191(10.7%)
 27  218.8   45.70   5.666  0.1466  184->190(27.9%) 186->191(25.5%)
 28  217.8   45.91   5.693  0.3156  183->189(31.4%) 184->190(28.0%) 187->197(13.8%)
 29  216.9   46.11   5.717  0.0744  182->189(58.3%)
 30  215.8   46.34   5.746  0.0045  186->192(71.0%)
 31  214.1   46.70   5.790  0.0789  181->189(53.3%)
 32  213.9   46.75   5.797  0.0023  187->198(70.6%)
 33  213.8   46.77   5.799  0.0059  185->193(59.8%)
 34  213.6   46.82   5.805  0.0110  182->192(25.4%) 183->190(20.3%) 181->189(12.0%)
 35  213.3   46.87   5.812  0.1888  182->192(37.0%) 183->190(17.6%)
 36  212.7   47.01   5.829  0.0001  184->196(92.1%)
 37  211.1   47.36   5.872  0.0139  184->191(28.3%) 183->190(16.9%) 184->190(13.8%)
 38  209.5   47.74   5.918  0.0044  177->188(81.3%)
 39  208.6   47.93   5.943  0.0030  169->188(59.1%) 167->188(16.1%)
 40  208.4   47.99   5.950  0.0181  175->188(50.4%) 176->188(16.5%)
```

Table S6. AuABTF1: Summary of calculated electronic transitions to Franck-Condon triplet states.

HOMO = 187; LUMO = 188

```
  #    nm  1000 cm-1   eV     f     Assignment (excitations with contrib. greater than 10.0%)
  1  561.9   17.80   2.206  0.0000  187->188(77.6%)
  2  430.5   23.23   2.880  0.0000  186->188(46.2%) 187->189(28.4%)
  3  363.3   27.53   3.413  0.0000  184->188(39.0%) 184->191(10.2%)
  4  332.6   30.07   3.728  0.0000  187->190(38.5%) 184->188(18.9%)
  5  329.0   30.40   3.769  0.0000  187->190(20.1%) 181->190(10.7%)
  6  325.9   30.68   3.804  0.0000  181->188(19.1%) 187->189(17.2%) 184->188(15.6%) 186-
>188(13.3%)
  7  319.0   31.35   3.887  0.0000  185->188(70.1%) 185->189(19.4%)
  8  317.3   31.51   3.907  0.0000  183->188(40.3%) 181->188(23.0%)
  9  307.3   32.55   4.035  0.0000  181->188(32.2%) 183->188(21.9%) 187->189(13.8%)
 10  305.5   32.73   4.058  0.0000  184->191(24.7%)
```

Table S7. AuABTF2: Summary of calculated electronic transitions to Franck-Condon singlet states.

HOMO = 215; LUMO = 216

```
  #    nm  1000 cm-1   eV     f     Assignment (excitations with contrib. greater than 10.0%)
  1  403.7   24.77   3.071  1.8963  215->216(97.1%)
  2  316.6   31.59   3.917  0.0000  213->216(81.6%) 213->217(11.6%)
  3  310.8   32.18   3.990  0.1193  215->217(89.3%)
  4  305.8   32.70   4.054  0.2069  214->216(87.0%)
  5  299.4   33.40   4.141  0.0030  215->220(33.8%) 212->216(26.2%) 215->221(17.6%)
  6  293.7   34.04   4.221  0.0278  212->216(58.4%)
  7  283.5   35.27   4.373  0.0355  210->216(59.4%) 215->226(13.9%) 207->216(12.8%)
  8  277.5   36.03   4.468  0.0006  215->218(96.7%)
  9  277.3   36.06   4.471  0.0000  215->219(96.4%)
 10  273.0   36.63   4.542  0.0467  215->221(53.1%) 215->220(39.2%)
 11  269.6   37.10   4.599  0.0004  215->222(93.6%)
 12  269.3   37.13   4.603  0.0129  211->216(84.7%) 211->217(13.8%)
 13  266.0   37.60   4.662  0.0184  207->216(51.6%) 215->221(17.8%) 210->216(12.3%)
 14  263.3   37.97   4.708  0.0012  213->217(80.4%) 213->216(11.9%)
 15  260.9   38.33   4.752  0.0365  215->223(72.0%)
 16  258.6   38.67   4.794  0.0004  215->224(88.7%)
 17  256.0   39.06   4.843  0.0002  202->216(91.5%)
 18  251.1   39.83   4.938  0.0034  209->216(38.8%) 206->216(26.5%) 208->216(14.5%)
 19  250.7   39.88   4.945  0.0075  215->228(75.7%)
 20  250.2   39.97   4.956  0.0025  208->216(73.1%) 209->216(23.3%)
 21  249.6   40.07   4.968  0.0128  209->216(32.7%) 206->216(28.1%)
 22  247.8   40.35   5.003  0.1116  215->226(54.8%) 206->216(13.1%)
 23  246.0   40.64   5.039  0.0167  211->217(71.4%) 211->216(13.1%)
 24  244.3   40.93   5.075  0.0764  214->217(72.1%)
 25  241.1   41.48   5.143  0.0045  215->225(89.1%)
 26  236.6   42.26   5.239  0.0004  205->216(24.7%) 208->219(14.5%) 205->217(10.4%)
 27  235.5   42.46   5.265  0.0001  215->229(83.9%) 214->229(12.4%)
```

```
 28  235.1    42.53   5.273  0.0061  209->219(19.0%) 213->218(18.7%) 205->218(14.0%) 208-
>222(12.8%)
 29  234.1    42.72   5.297  0.0445  214->220(37.8%) 212->217(10.0%)
 30  233.7    42.78   5.304  0.0014  213->220(63.9%)
 31  233.6    42.81   5.307  0.0001  205->216(68.3%)
 32  232.7    42.97   5.327  0.0011  213->219(96.5%)
 33  232.4    43.03   5.335  0.0060  215->227(97.7%)
 34  232.3    43.05   5.338  0.0052  213->221(51.7%) 213->226(14.4%)
 35  232.1    43.08   5.342  0.0051  213->218(71.5%)
 36  231.4    43.22   5.359  0.0208  203->216(52.9%) 206->216(14.0%)
 37  229.2    43.63   5.409  0.0253  212->217(23.7%) 214->223(21.0%) 214->220(15.3%) 203-
>216(13.2%)
 38  228.8    43.71   5.420  0.0112  204->216(85.9%)
 39  228.3    43.80   5.430  0.0383  215->230(51.2%)
 40  227.0    44.05   5.462  0.0359  213->222(84.0%)
```

Table S8. AuABTF2: Summary of calculated electronic transitions to Franck-Condon triplet states.

HOMO = 215; LUMO = 216

```
  #    nm  1000 cm-1   eV     f     Assignment (excitations with contrib. greater than 10.0%)
  1  569.7    17.55   2.176  0.0000  215->216(76.7%)
  2  433.0    23.09   2.863  0.0000  214->216(44.6%) 215->217(20.1%)
  3  363.8    27.49   3.408  0.0000  212->216(33.7%) 212->223(11.0%)
  4  353.6    28.28   3.506  0.0000  208->218(21.6%) 205->222(17.8%) 204->219(14.9%)
  5  336.8    29.69   3.681  0.0000  215->221(23.9%) 215->220(15.4%) 215->217(10.5%) 214-
>216(10.0%)
  6  334.3    29.91   3.708  0.0000  212->216(35.0%) 207->216(19.0%)
  7  328.2    30.47   3.778  0.0000  213->216(70.9%) 213->217(16.1%)
  8  324.6    30.80   3.819  0.0000  215->220(22.5%)
  9  318.3    31.41   3.895  0.0000  210->216(39.3%) 207->216(26.0%)
 10  313.7    31.88   3.953  0.0000  215->217(23.2%)
```

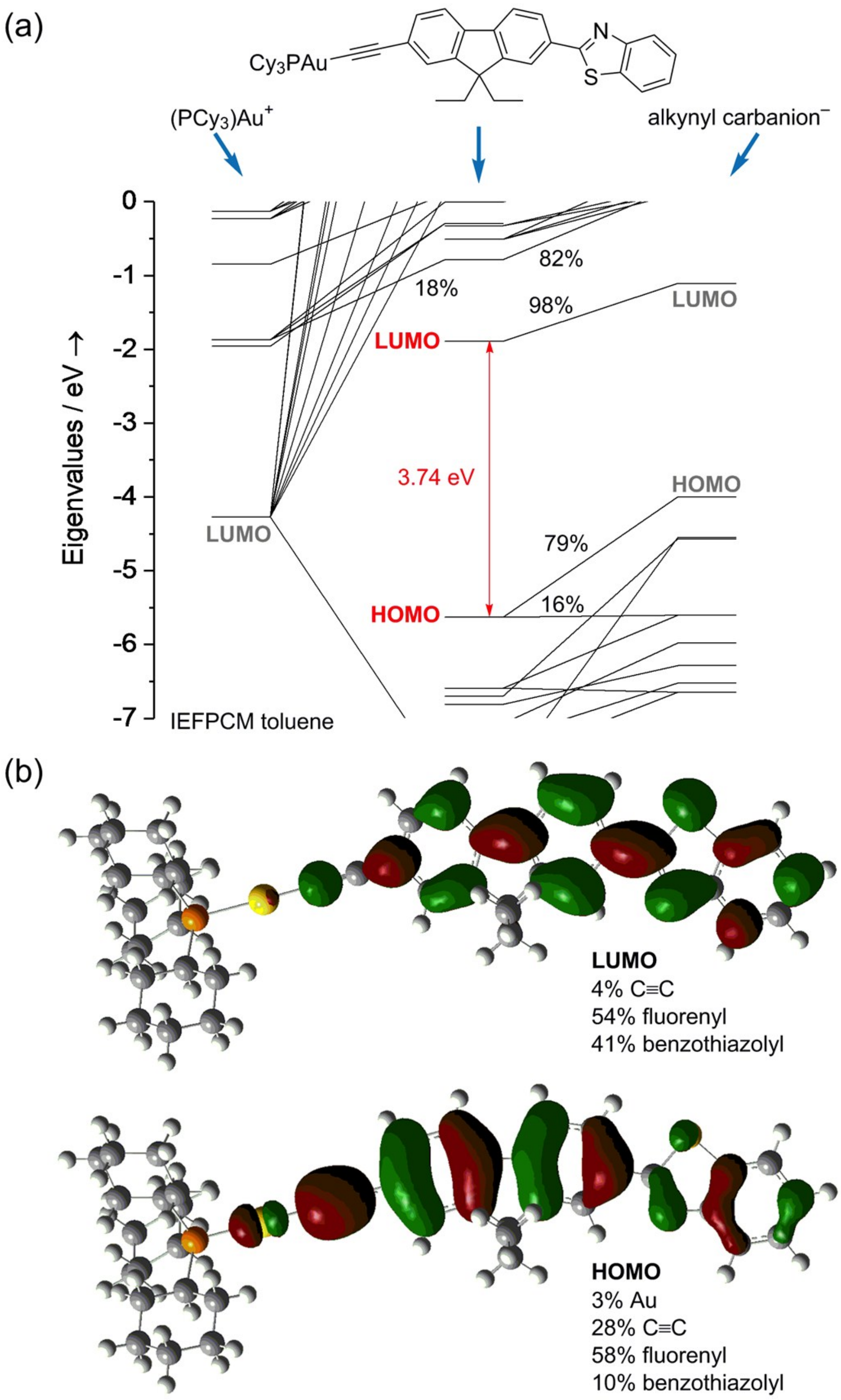

Figure S18: (a) Frontier orbital energy diagram of **Au-ABTF1**. (b) Kohn-Sham orbital plots (HOMO and LUMO) for **Au-ABTF1**. (Percentages are of electron density)

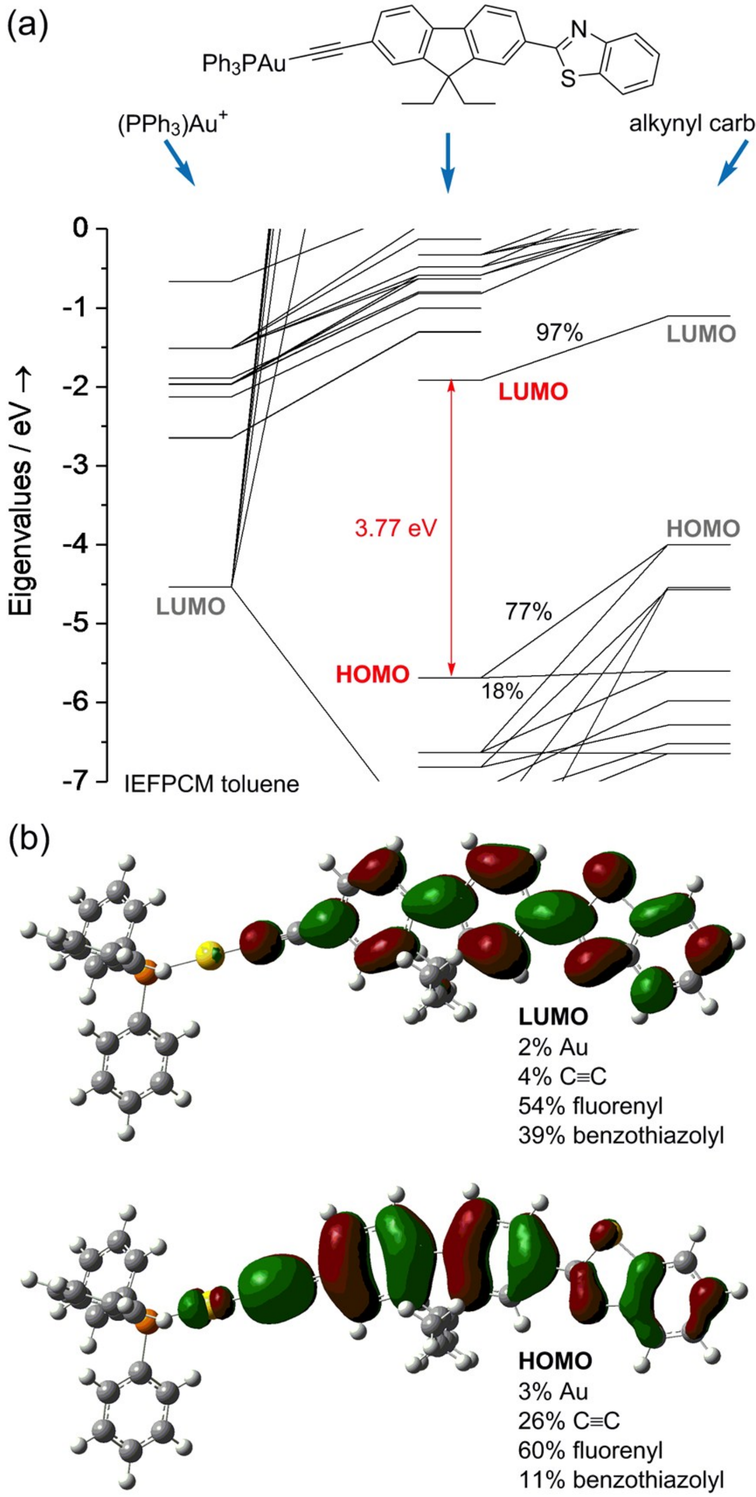

Figure S19: (a) Frontier orbital energy diagram of **Au-ABT0**. (b) Kohn-Sham orbital plots (HOMO and LUMO) for **Au-ABTF0**. (Percentages are of electron density)

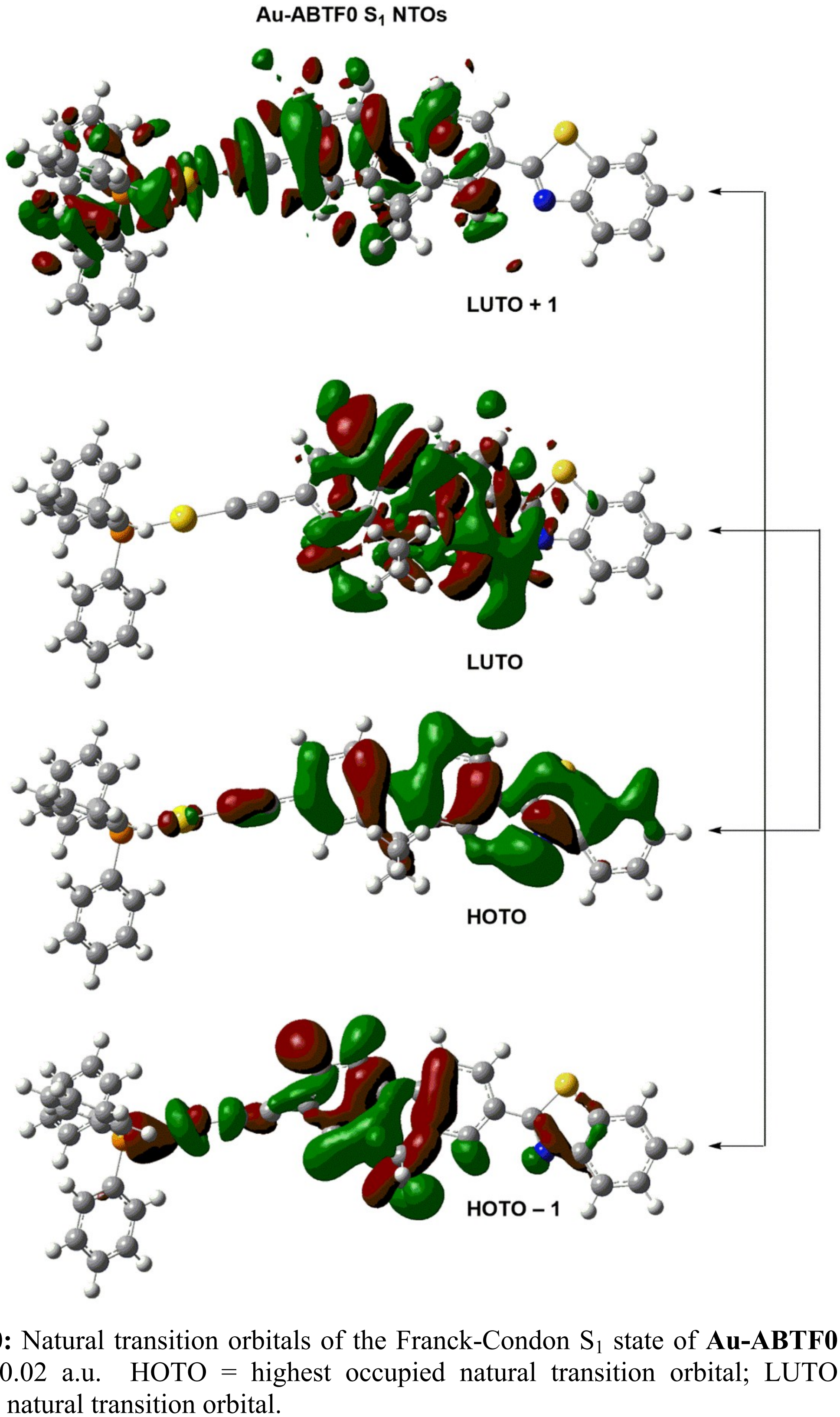

Figure S20: Natural transition orbitals of the Franck-Condon S_1 state of **Au-ABTF0**. Contour levels are 0.02 a.u. HOTO = highest occupied natural transition orbital; LUTO = lowest unoccupied natural transition orbital.

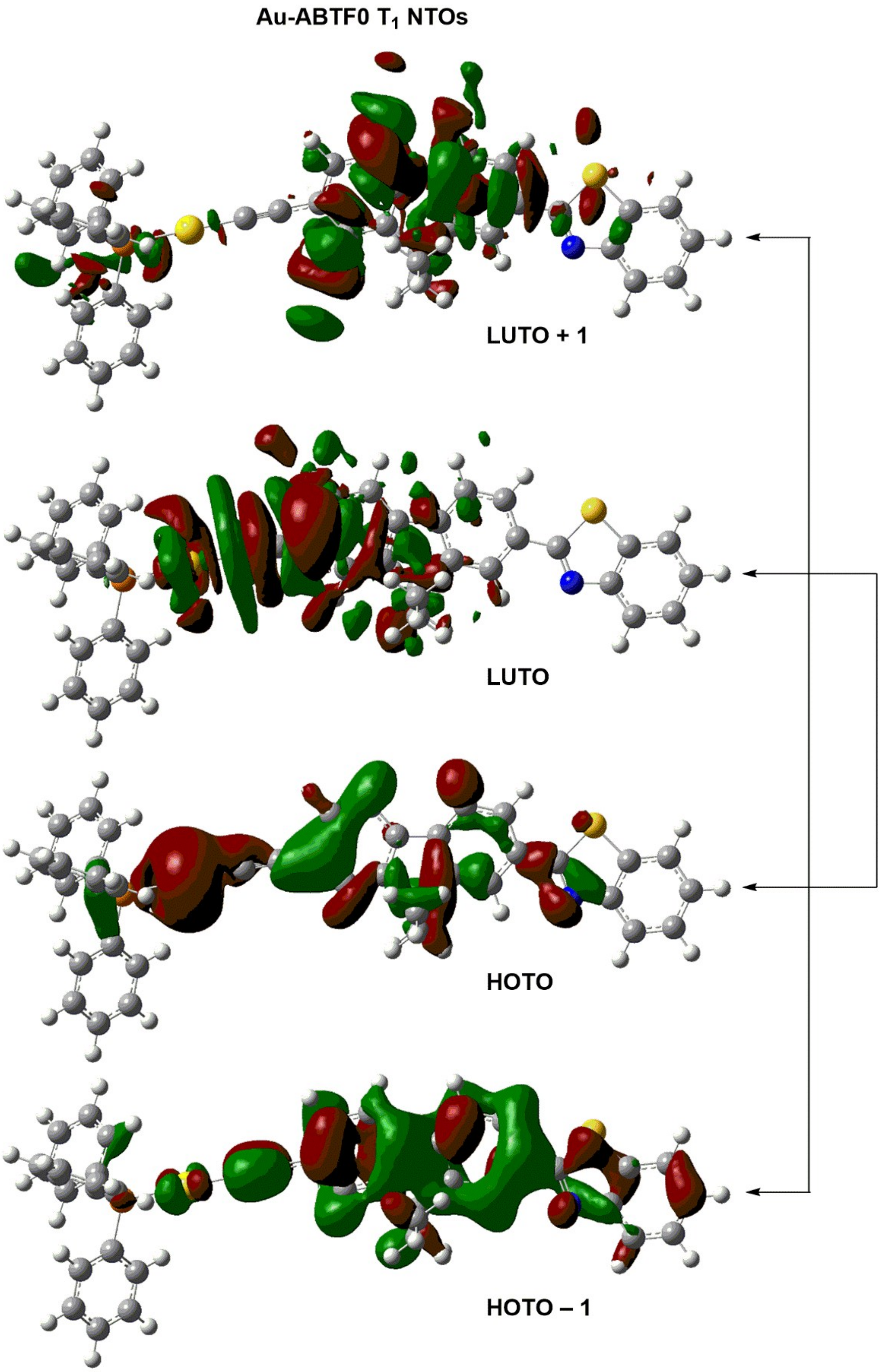

Figure S21: Natural transition orbitals of the Franck-Condon T_1 state of **Au-ABTF0**. Contour levels are 0.02 a.u. HOTO = highest occupied natural transition orbital; LUTO = lowest unoccupied natural transition orbital.

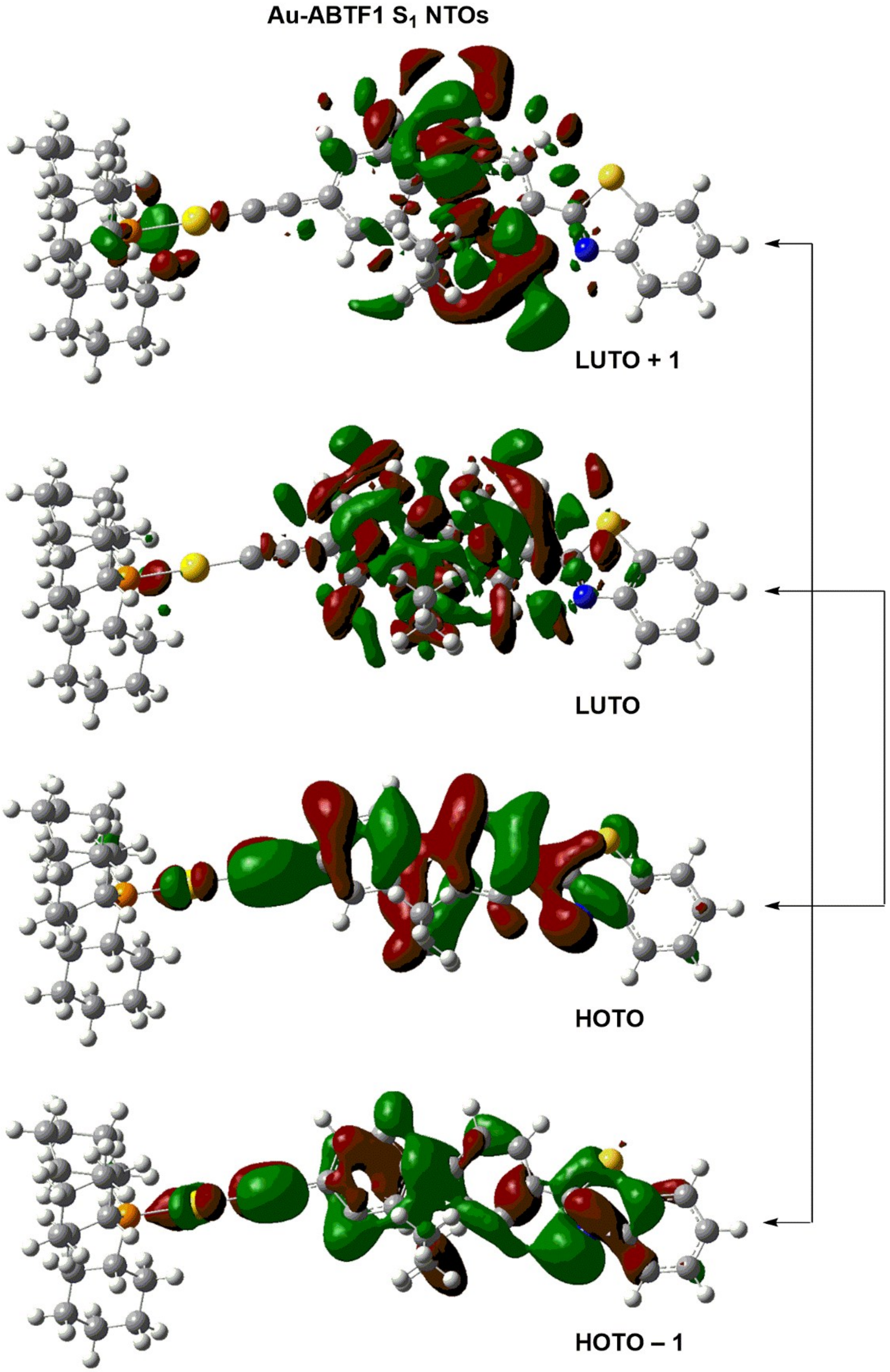

Figure S22: Natural transition orbitals of the Franck-Condon S_1 state of **Au-ABTF1**. Contour levels are 0.02 a.u. HOTO = highest occupied natural transition orbital; LUTO = lowest unoccupied natural transition orbital.

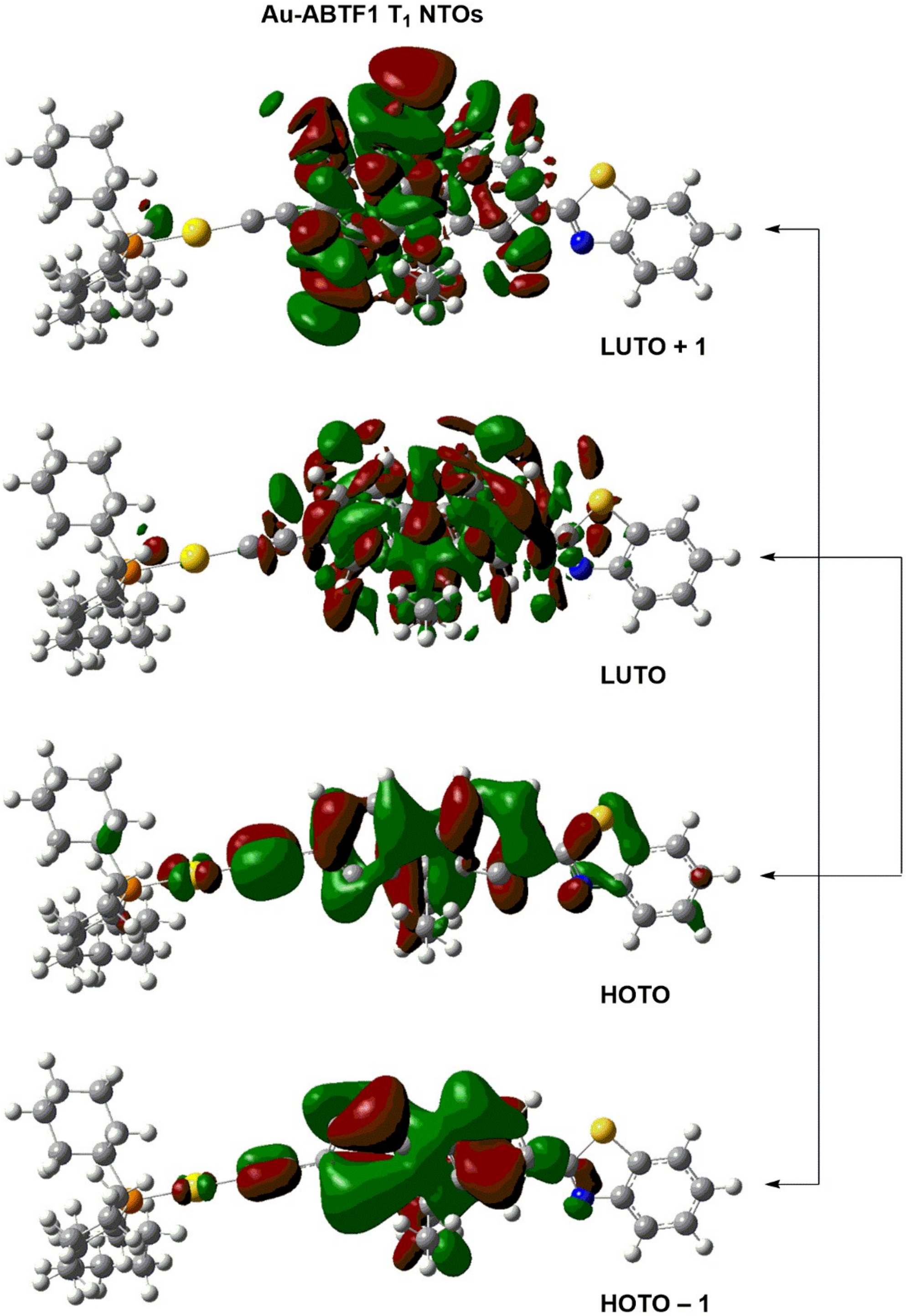

Figure S23: Natural transition orbitals of the Franck-Condon T_1 state of **Au-ABTF1**. Contour levels are 0.02 a.u. HOTO = highest occupied natural transition orbital; LUTO = lowest unoccupied natural transition orbital.

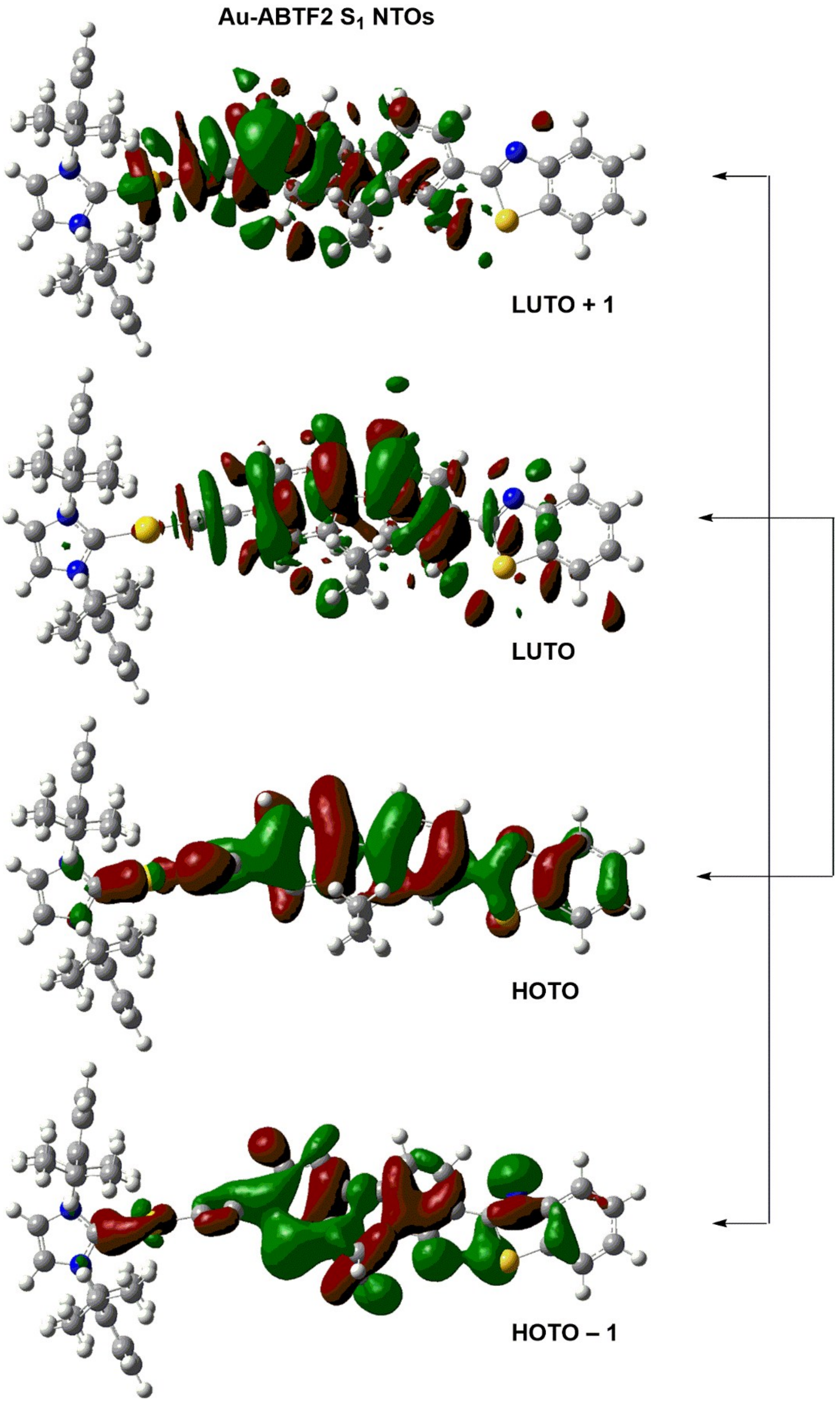

Figure S24: Natural transition orbitals of the Franck-Condon S_1 state of **Au-ABTF2**. Contour levels are 0.02 a.u. HOTO = highest occupied natural transition orbital; LUTO = lowest unoccupied natural transition orbital.

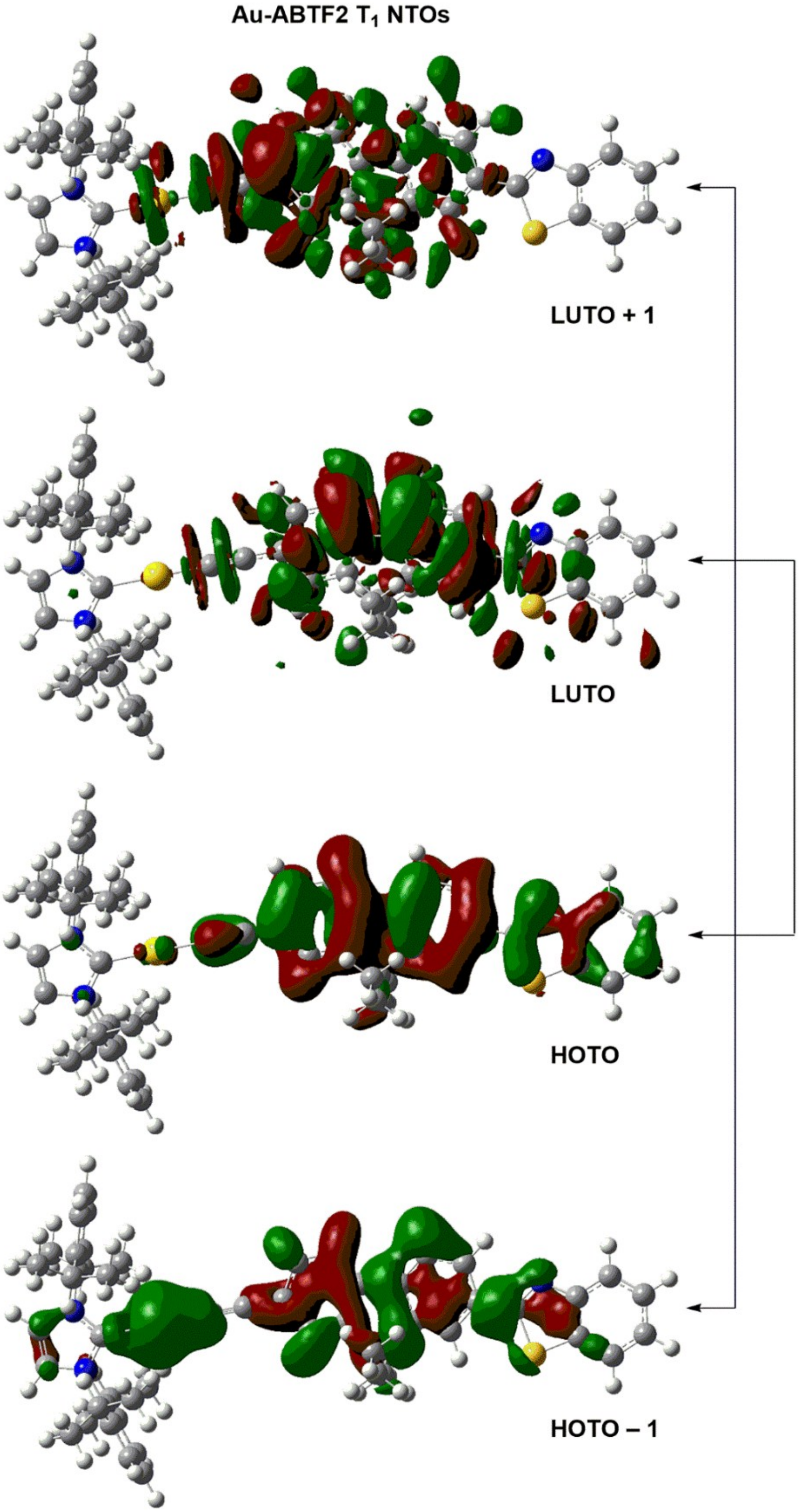

Figure S25: Natural transition orbitals of the Franck-Condon T$_1$ state of **Au-ABTF2**. Contour levels are 0.02 a.u. HOTO = highest occupied natural transition orbital; LUTO = lowest unoccupied natural transition orbital.

VI. References

1 D. V Partyka, T. J. Robilotto, M. Zeller, A. D. Hunter and T. G. Gray, Dialkylbiarylphosphine Complexes of Gold(I) Halides. Gold−Aryl π-Interactions in the Solid State, *Organometallics*, 2008, **27**, 28–32.

2 J. E. Rogers, J. E. Slagle, D. M. Krein, A. R. Burke, B. C. Hall, A. Fratini, D. G. McLean, P. A. Fleitz, T. M. Cooper, M. Drobizhev, N. S. Makarov, A. Rebane, K. Y. Kim, R. Farley and K. S. Schanze, Platinum acetylide two-photon chromophores, *Inorg. Chem.*, 2007, **46**, 6483–6494.

3 J. J. Mihaly, D. J. Stewart, T. A. Grusenmeyer, A. T. Phillips, J. E. Haley, M. Zeller and T. G. Gray, Photophysical properties of organogold(i) complexes bearing a benzothiazole-2,7-fluorenyl moiety: Selection of ancillary ligand influences white light emission, *Dalt. Trans.*, 2019, **48**, 15917–15927.

4 A. T. Phillips, Z. Yu, D. J. Stewart, T. M. Cooper, J. E. Haley, L.-S. Tan and T. A. Grusenmeyer, Influence of Structural Isomerism on the Photophysical Properties of a Series of Donor–Acceptor 1-Naphthalenecarbonitrile Derivatives Possessing Amine Substituents, *J. Phys. Chem. A*, 2020, **124**, 2113–2122.

5 A. V Nikolaitchik, O. Korth and M. A. J. Rodgers, Crown Ether Substituted Monomeric and Cofacial Dimeric Metallophthalocyanines. 1. Photophysical Studies of the Free Base, Zinc(II), and Copper(II) Variants, *J. Phys. Chem. A*, 1999, **103**, 7587–7596.

6 F. Wilkinson, W. P. Helman and A. B. Ross, Quantum Yields for the Photosensitized Formation of the Lowest Electronically Excited Singlet State of Molecular Oxygen in Solution, *J. Phys. Chem. Ref. Data*, 1993, **22**, 113–262.

7 A. M. Brouwer, *Pure Appl. Chem.*, 2011, 83, 2213.

8 M. Montalti, A. Credi, L. Prodi and M. Teresa Gandolfi, *Handbook of Photochemistry, Third Edition*, CRC Press, 3rd Editio., 2006.

9 I. Carmichael and G. L. Hug, Triplet–Triplet Absorption Spectra of Organic Molecules in Condensed Phases, *J. Phys. Chem. Ref. Data*, 1986, **15**, 1–250.

10 C. Creutz, M. Chou, T. L. Netzel, M. Okumura and N. Sutin, Lifetimes, Spectra, and Quenching of the Excited States of Polypyridine Complexes of Iron(II), Ruthenium(II), and Osmium(II), *J. Am. Chem. Soc.*, 1980, **102**, 1309–1319.

11 T. N. Singh-Rachford and F. N. Castellano, Photon upconversion based on sensitized triplet–triplet annihilation, *Coord. Chem. Rev.*, 2010, **254**, 2560–2573.

12 G. M. Sheldrick, A short history of SHELX, *Acta Crystallogr. Sect. A*, 2008, **64**, 112–122.

13 G. M. Sheldrick, Crystal structure refinement with SHELXL, *Acta Crystallogr. Sect. C*, 2015, **71**, 3–8.

14 C. B. Hübschle, G. M. Sheldrick and B. Dittrich, ShelXle: a Qt graphical user interface for SHELXL, *J. Appl. Crystallogr.*, 2011, **44**, 1281–1284.

15 L. Krause, R. Herbst-Irmer, G. M. Sheldrick and D. Stalke, Comparison of silver and molybdenum microfocus X-ray sources for single-crystal structure determination, *J. Appl. Crystallogr.*, 2015, **48**, 3–10.

16 S. Parsons, H. D. Flack and T. Wagner, Use of intensity quotients and differences in absolute structure refinement, *Acta Crystallogr. Sect. B*, 2013, **69**, 249–259.

17 Gaussian 16, Revision A.03, M. J. Frisch, G. W. Trucks, H. B. Schlegel, G. E. Scuseria, M. A. Robb, J. R. Cheeseman, G. Scalmani, V. Barone, G. A. Petersson, H. Nakatsuji, X. Li, M. Caricato, A. V Marenich, J. Bloino, B. G. Janesko, R. Gomperts, B. Mennucci, H. P. Hratchian, J. V Ortiz, A. F. Izmaylov, J. L. Sonnenberg, D. Williams-Young, F. Ding, F. Lipparini, F. Egidi, J. Goings, B. Peng, A. Petrone, T. Henderson, D. Ranasinghe, V. G. Zakrzewski, J. Gao, N. Rega, G. Zheng, W. Liang, M. Hada, M. Ehara, K. Toyota, R. Fukuda, J. Hasegawa, M. Ishida, T. Nakajima, Y. Honda, O. Kitao, H. Nakai, T. Vreven, K. Throssell, J. A. Montgomery Jr., J. E. Peralta, F. Ogliaro, M. J. Bearpark, J. J. Heyd, E. N. Brothers, K. N. Kudin, V. N. Staroverov, T. A. Keith, R. Kobayashi, J. Normand, K. Raghavachari, A. P. Rendell, J. C. Burant, S. S. Iyengar, J. Tomasi, M. Cossi, J. M. Millam, M. Klene, C. Adamo, R. Cammi, J. W. Ochterski, R. L. Martin, K. Morokuma, O. Farkas, J. B. Foresman and D. J. Fox, Gaussian, Inc., Wallingford CT, 2016.

18 M. Dolg, U. Wedig, H. Stoll and H. Preuss, Energy-adjusted ab initio pseudopotentials for the first row transition elements, *J. Chem. Phys.*, 1987, **86**, 866–872.

19 J. P. Perdew, K. Burke and M. Ernzerhof, Generalized Gradient Approximation Made Simple, *Phys. Rev. Lett.*, 1996, **77**, 3865–3868.

20 N. Godbout, D. R. Salahub, J. Andzelm and E. Wimmer, Optimization of Gaussian-type basis sets for local spin density functional calculations. Part I. Boron through neon, optimization technique and validation, *Can. J. Chem.*, 1992, **70**, 560–571.

21 S. Miertuš, E. Scrocco and J. Tomasi, Electrostatic interaction of a solute with a continuum. A direct utilizaion of AB initio molecular potentials for the prevision of solvent effects, *Chem. Phys.*, 1981, **55**, 117–129.

22 J. Tomasi, B. Mennucci and R. Cammi, Quantum Mechanical Continuum Solvation Models, *Chem. Rev.*, 2005, **105**, 2999–3094.

23 E. Cancès, B. Mennucci and J. Tomasi, A new integral equation formalism for the polarizable continuum model: Theoretical background and applications to isotropic and anisotropic dielectrics, *J. Chem. Phys.*, 1997, **107**, 3032–3041.

24 B. Mennucci, E. Cancès and J. Tomasi, Evaluation of Solvent Effects in Isotropic and Anisotropic Dielectrics and in Ionic Solutions with a Unified Integral Equation Method: Theoretical Bases, Computational Implementation, and Numerical Applications, *J. Phys. Chem. B*, 1997, **101**, 10506–10517.

25 S. I. Gorelsky and A. B. P. Lever, Electronic structure and spectra of ruthenium diimine complexes by density functional theory and INDO/S. Comparison of the two methods, *J. Organomet. Chem.*, 2001, **635**, 187–196.

26 S. I. Gorelsky, AOMix: Program for Molecular Orbital Analysis, http://www.sg-chem.net.